Mon. Not. R. Astron. Soc. **000**, 000–000 (0000) Printed 27 December 2011 (MN LATEX style file v2.2)

Linking Double-peaked Narrow-Line AGN and Dual Supermassive Black Holes in Galaxy Merger Simulations

Laura Blecha, Abraham Loeb, & Ramesh Narayan

27 December 2011

ABSTRACT

Recent observational searches for supermassive black hole (SMBH) pairs have made great progress by focusing on the kiloparsec-scale phase of SMBH pair evolution in mergers. Spectroscopic surveys have found that about 1% of active galactic nuclei (AGN) have double-peaked narrow [OIII] lines, possibly indicating BH orbital motion on approximately kiloparsec scales; this has greatly increased the number of candidate SMBH pairs. Follow-up imaging has already provided evidence that $\gtrsim$ 10% of these are strong candidates. On the theoretical side, however, little has been done to understand the nature of double-peaked narrow-line (NL) AGN and their relation to BHs in merging galaxies. We present a first attempt to model the NL region in hydrodynamic simulations of galaxy mergers, using a semi-analytic model. We find that double-peaked NLs induced by BH motion are a fairly generic but short-lived feature of major mergers, indicating that most comparable-mass dual SMBHs should pass through this phase. Double-peaked NL AGN are most likely to be observed in late-stage galaxy mergers, during the kpc-scale phase or soon after the BH merger. However, even in the kpc-scale phase, a *minority* of double-peaked NLs are directly induced by BH motion; the rest are produced by gas kinematics such as rotation, though these still may be influenced by the BH motion. Further, some of the double-peaked NLs induced by BH motion have small projected separations, $\sim 0.1-1$ kpc, indicating that a dual BH may not easily be confirmed or excluded via imaging in these cases. Galaxies exhibiting morphological signatures of a late-stage merger provide additional, indirect evidence for the presence of a dual BH, though the morphology will be similar in the post-BH-merger phase. Double-peaked NL AGN spectra with large peak velocity splitting ($\gtrsim$500 km s^{-1}) or with a discernible overall velocity shift are more likely to contain dual AGN, but again these signatures could also be produced after the BH merger by gas or BH motion in the rapidly-deepening central potential well of a gas-rich merger remnant. The lifetime of double-peaked NL activity is strongly dependent on viewing angle, often varying by at least an order of magnitude for different sight lines, and also depends on the conditions of the merging galaxy. Gas-rich mergers between nearly equal mass galaxies have more NL AGN activity, though these AGN may more often be obscured. Our results support the notion that selection of double-peaked NL AGN is a promising method for identifying dual BH candidates, but demonstrate the critical importance of high-resolution, multi-wavelength follow-up observations, and the use of multiple lines of evidence, for confirming the dual nature of candidate BH pairs.

1 INTRODUCTION

Although supermassive black hole (SMBH) pairs are a natural result of major galaxy mergers, until recently, evidence for their existence has been scarce. On large scales, when the BHs simply follow the motion of their host galaxies, some constraints are obtained from quasar clustering surveys. About 0.1% of quasars are known to be in pairs on scales of $\sim$ 100 kpc (Hennawi et al. 2006); however, on these large scales it is unclear whether nuclear activity is actually associated with galaxy interactions. When the galaxies are in later stages of merging and the BH separation is $\sim 1-10$ kpc, dynamical friction drives the evolution of the BH pair toward the center of the merger remnant. This "kiloparsec-scale" phase has seen by far the most recent progress in identification of candidate SMBH pairs. A handful of spatially-resolved AGN pairs on these scales have been found (Komossa et al. 2003; Bianchi et al. 2008; Green et al. 2010; Koss et al. 2011a), and, notably, a candidate BH pair with $\sim$ 150 pc separation was recently discovered (Fabbiano et al. 2011). Recently, however, multiple spectroscopic surveys of AGN have found consistently that about 1% of all AGN have double-peaked narrow [O III] lines, a possible signature of SMBH orbital motion on kpc scales (Comerford et al. 2009; Smith et al. 2010; Liu et al. 2010b). This finding has increased the number of candidate SMBH pairs to several hundred. While only a fraction of these double-peaked narrow-line (dNL) AGN are actually expected to contain SMBH pairs, follow-up observations have already revealed strong evidence that some of these are in fact dual SMBHs. Observations of dNL AGN that combine high-resolution ground-based optical and near-infrared imaging with long-slit spectroscopy (Liu et al. 2010a; Shen et al. 2011) or integral field unit (IFU) data (Fu et al. 2011b; McGurk et al. 2011) have revealed

numerous systems with two resolved stellar components in images that correspond with the spatial positions of the two emission components in their spectra. These are among the most compelling dual BH candidates. Shen et al. (2011) estimate that 10-50% of dNL AGN host dual BHs, and that, when corrected for sample completeness, 0.5-2.5% of $z < 0.30$ Type 2 AGN are active, kpc-scale BH pairs. Additionally, Fu et al. (2011a) and Rosario et al. (2011) have used adaptive optics (AO) imaging to constrain the environment and host galaxy morphology of a subset of the dNL AGN; their estimates of the dual BH fraction are in broad agreement with those of Shen et al. (2011). Comerford et al. (2011a) have conducted analysis of 81 slit spectra obtained for dNL AGN; they find that *all* of these systems show spatially-separated emission components on $\sim$ kpc scales. Many (42%) also show extended emission components; Comerford et al. (2011a) suggest that these are less promising candidates, because their double-peaked features may arise from outflows. Still more compelling evidence for dual BHs comes from the detection of a dual compact X-ray (Comerford et al. 2011b) and radio (Fu et al. 2011c) source, respectively, in two dNL AGN. In contrast, Rosario et al. (2010) combined slit spectroscopy with VLA imaging to demonstrate that the dual BH scenario is *disfavored* in two systems where radio jets are likely responsible for the double-peaked spectral features. In summary, we see that while follow-up observations are required to confirm dual BH candidates, the selection of AGN with double-peaked spectra has already led to a substantial increase in the number of known candidate BH pairs.

On smaller scales ($\lesssim 10$ pc), BH pairs evolve to form a true bound binary BH. These present a formidable challenge for observers, partly because they are difficult if not impossible to resolve. Additionally, there is still an uncertainty regarding the timescale required for the binary to evolve from scales of a few pc down to parsec scales where GW emission dominates the orbital decay. It has been shown that in highly symmetric, spheroidal galaxies with little to no gas, BH binaries may "stall" at $\sim$ 1 pc for more than a Hubble time (e.g., Begelman et al. 1980; Milosavljević & Merritt 2001; Yu 2002) – i.e., they never reach the final, GW-driven phase of merging. If the galaxy is gas-rich or substantially triaxial, however, the BHs may merge on a much shorter timescale ($\sim 10^6 - 10^7$ yr from the hard binary stage; e.g., Gerhard & Binney 1985; Yu 2002; Berczik et al. 2006; Escala et al. 2004; & Miralda-Escude 1997). Only one confirmed example of a bound SMBH binary is known, with a 7 pc separation (Rodriguez et al. 2006). Numerous sub-parsec (spectroscopic) binary candidates have been proposed, but confirming their binary nature will likely require a better understanding of broad line physics (Dotti et al. 2008; Bogdanović et al. 2009; Boroson & Lauer 2009; Tsalmantza et al. 2011; Eracleous et al. 2011). Therefore, the kiloparsec-scale phase of BH pair evolution currently seems to be the most promising avenue for studies of dual SMBHs.

Theoretical studies of SMBH mergers face their own challenges, largely owing to the vast range in physical scales involved. Significant progress has been made on the smallest scales; simulations of BH mergers using full general relativity are now possible and can generate precise waveforms of GW emission as well as the remnant BH properties (e.g., Pretorius 2005; Campanelli et al. 2006; Baker et al. 2006). On galactic scales, interactions and mergers have been studied extensively with hydrodynamic simulations (e.g. Matteo et al. 2005; Robertson et al. 2006; Hopkins et al. 2006). In relative terms, BH evolution on intermediate scales is poorly understood, although as illustrated above this regime is currently the most active focus of observational studies. In particular, little has been done to understand the nature of double-peaked narrow-line (NL) AGN. Galaxy merger simulations have not considered the NL region (NLR), and detailed photoionization models have not been applied to the rapidly-varying environment of a late-stage merger. Here, we make a first attempt to model the NLR during galaxy mergers using hydrodynamic simulations, with special attention to the kiloparsec-scale phase that may produce double-peaked NL AGN.

This paper is organized as follows. In § 2.1 & 2.2, we describe our simulations and galaxy merger models. Our semianalytic model for the narrow-line gas, which is implemented in post-processing, is detailed in § 2.3 - § 2.4. Our results are presented in § 3. In § 3.1, we describe the evolution of the NLR throughout a major merger and discuss dependence on merger parameters. We describe the morphological properties of the NLRs in § 3.2, and in § 3.3 we explore the observable signatures of kiloparsec-scale double-NL AGN. The lifetimes of double-NL AGN are discussed in § 3.4. Finally, we summarize and discuss our results in § 4. Throughout the paper, we assume a flat ΛCDM cosmology with $H_0 = 71$ km s^{-1} Mpc^{-1}, $\Omega_{\rm m} = 0.27$, and $\Omega_\Lambda = 0.73$.

2 METHODS

2.1 Simulations

We use GADGET-3 for our numerical studies of SMBH mergers. GADGET is a smoothed-particle hydrodynamics (SPH) code that conserves both energy and entropy (Springel 2005). The version we use includes radiative cooling as well as a sub-resolution model for a multiphase interstellar medium (ISM, Springel & Hernquist 2003) that accounts for star formation and supernova feedback. In addition, the code models BHs as gravitational "sink" particles that contain a BH seed and a gas reservoir. The reservoir is replenished by stochastic accretion of neighboring gas particles, but the actual accretion rate onto the BH is calculated smoothly using the Bondi-Hoyle formula (Bondi & Hoyle 1944) with locally-averaged values for the density and sound speed. The accretion rate is modified by a multiplicative factor to account for the increase in density and sound speed that should occur on sub-resolution scales near the BH accretion disk; we adopt a standard value of 100. We include a model for thermal feedback from the BH by assuming that 5% of the luminous output from the BH is coupled to the surrounding gas particle as thermal energy. We note that this model does not allow for the possibility of AGN outflows, and thus we are unable to model this possible mechanism for producing some double-peaked spectral features in AGN. Angular momentum is conserved during accretion of gas particles, but because this is a stochastic process we also introduce an accretion drag force calculated from the Bondi accretion rate. These prescriptions are described in more detail in Springel et al. (2005).

2.2 Galaxy and BH Merger Models

The progenitor galaxies for our merger simulations consist of a dark matter halo, a disk of gas and stars, and a central BH sink particle as described above. We also include a stellar bulge component in some models. In each case the total mass of the primary galaxy is 1.36×10^{12} M$_\odot$, and 4.1% of this mass is in baryons. We simulate major galaxy mergers with mass ratios of q =1, 0.5, & 0.333, and the initial gas fraction by mass of the disk is varied between 4 and 30%. We use fairly high mass and spatial resolution in order

to resolve as best as possible the NLR around each BH. The gravitational softening length adopted is $r_{\rm soft} = 37$ pc for baryons and $r_{\rm soft,DM} = 111$ pc for dark matter, and the particle masses for each particle type are $m_{\rm star} = 4.2 \times 10^4$ M$_\odot$, $m_{\rm gas} = 2.8 \times 10^4$ M$_\odot$, and $m_{\rm DM} = 5.4 \times 10^5$ M$_\odot$.

Each galaxy is given a single BH with a seed mass of 1.43×10^5 M$_\odot$; the small value chosen reflects the fact that in most cases our galaxies are initially bulgeless. We use the same BH merger prescription as in Blecha et al. (2011), in that the BH merger time ($t_{\rm mrg}$) is determined based on the BH separation ($a_{\rm sep}$) and relative velocity ($v_{\rm rel}$), and then the simulation is restarted at an earlier point to merge the BHs at that exact time. We define $t_{\rm mrg}$ as the time at which $a_{\rm sep} < r_{\rm soft}$ and $v_{\rm rel} < 0.5 c_{\rm sound}$. Restarting the simulations is particularly important for our present study, because a detailed analysis of the short-lived kpc-scale phase of BH evolution requires good time resolution. In order to provide this resolution where needed without generating excessive data in the early merger phase, we run the initial simulations with a time resolution (snapshot output frequency) of 10 Myr, and restart the simulation 100 Myr before the kpc-scale phase (as defined below) with a time resolution of 1 Myr. The galaxies are set on an inclined, parabolic orbit with an initial separation and impact parameter of 143 kpc and 7.1 kpc, respectively.

2.3 NLR Identification

Here we outline a basic procedure for determining the location, kinematics, and (Hβ) luminosity of the narrow-line region around one or more AGN in a gaseous galaxy merger simulation with GADGET-3 . All of the calculations described here are done in post-processing, i.e. after the GADGET simulation has finished.

2.3.1 BH accretion & luminosity

We use the standard GADGET prescription for BH accretion; i.e., the Bondi-Hoyle accretion rate, capped at the Eddington limit.

$$\dot{M} = \min(\dot{M}_{\rm Bondi}, \dot{M}_{\rm Edd}), \quad (1)$$

$$\dot{M}_{\rm Bondi} = \frac{4\pi (G M_{\rm BH})^2 \rho_{\rm g,\infty}}{(v_{\rm rel}^2 + c_{\rm s,\infty}^2)^{3/2}} \quad (2)$$

$$\dot{M}_{\rm Edd} = \frac{4\pi G M_{\rm BH}}{0.1 \kappa_{\rm es}\, c} \quad (3)$$

where $v_{\rm rel}$, $c_{\rm s,\infty}$, and $\rho_{\rm g,\infty}$ are all computed as averages over the gas particles neighboring the BH. The Eddington value assumes a radiative efficiency of 0.1. Using this accretion rate, we can calculate a bolometric luminosity

$$L_{\rm bol} = \eta \dot{M}\, c^2, \quad (4)$$

where the radiative efficiency η is assumed to be 0.1 unless $\dot{M} \ll \dot{M}_{\rm Edd}$, in which case the BH is assumed to be radiatively inefficient, with the following scaling for η (Narayan & McClintock 2008):

$$\eta = 0.1 \left(\frac{\dot{M}}{0.01 \dot{M}_{\rm Edd}} \right), \quad \dot{M} < 0.01 \dot{M}_{\rm Edd}. \quad (5)$$

2.3.2 Ionizing photon production rate

To calculate properties of the NL region, we need to know the number of ionizing photons produced by the accreting BHs. We begin by applying a reverse bolometric correction to $L_{\rm bol}$ to obtain the B-band luminosity, and then we assume a broken power-law form for the optical - UV spectrum. Following the method of Marconi et al (2004), the bolometric correction is:

$$\log \left(\frac{L_{\rm bol}}{\nu_{\rm B} L_{\nu_{\rm B}}} \right) = 0.8 - 0.067\mathcal{L} + 0.017\mathcal{L}^2 - 0.0023\mathcal{L}^3, \quad (6)$$

where $\mathcal{L} = \log L_{\rm bol} - 12$ and $L_{\rm bol}$ is in units of $L_\odot$. For the broken power-law, we use the following spectral indices from the AGN SED fits of Marconi et al. (2004):

$$\alpha_{\rm opt} = -0.44, \;\; 1\,\mu{\rm m} > \lambda > 1300\text{Å} \quad (7)$$

$$\alpha_{\rm UV} = -1.76, \;\; 1200\text{Å} > \lambda > 500\text{Å}. \quad (8)$$

Then we can get the normalization factor $A_{\rm opt}$ from the bolometric correction by taking $\nu_{\rm B} L_{\nu_{\rm B}} = A_{\rm opt} \nu_{\rm B}^{\alpha_{\rm opt}+1}$. To get the normalization for the UV range we can take $\nu L_\nu(1300\text{Å}) = \nu L_\nu(1200\text{Å})$, which gives

$$\frac{A_{\rm UV}}{A_{\rm opt}} = 2.02 \times 10^{20}. \quad (9)$$

The normalization $A_{\rm UV}$ allows us to calculate the number of ionizing photons emitted per unit time by the source:

$$Q = \int_{\nu_0}^{\infty} \frac{L_\nu}{h\nu} d\nu, \quad (10)$$

where $\nu_0 = 13.6$ eV.

2.3.3 Selection criterion for cold-phase gas

In order to determine which gas in the galactic center will be ionized by the radiation and produce narrow-line emission, we must impose selection criteria on the SPH particles. The multiphase model for the ISM in GADGET assumes that the gas is comprised of a "cold" phase and a "hot" phase, which can exchange mass via star formation, cooling, and evaporation from supernovae. First, we select only those gas particles that have a nonzero fraction of mass $f_{\rm cold}$ in the "cold" phase. We assume that the cold-phase gas has fragmented into discrete clouds on sub-resolution scales. The NL clouds are heated by photoionization and should be warmer than the cold clouds in the multiphase ISM ($\sim 10^4$ K versus $\sim 10^3$ K) and thus less dense (assuming pressure equilibrium between phases). Therefore, we use the parameters of the multiphase model only for selection of SPH particles that contain cold gas, and we instead calculate a "cloud density" for each of these particles: $\rho_{\rm cl} = \rho_{\rm sph} T_{\rm sph} / 10^4$ K. (Here, the subscript "sph" denotes that these quantities are averaged between the hot and cold phases, and the subscript "cl" denotes the quantities for our NL cloud model.)

2.3.4 Selection criterion for gas particle covering fraction

We also impose a criterion on the SPH particles such that the solid angle subtended by NL clouds does not exceed 4π. We cannot determine exactly which clouds will have unobscured sight lines to the AGN, as their size is below our resolution limit and our simulations do not include radiative transfer. However, we account for the problem of particle self-blocking in an average sense, as follows. An SPH particle that subtends a solid angle $\Omega_{\rm sph}$ has a covering fraction

$$f_{\Omega_{\rm sph}} = \frac{\Omega_{\rm sph}}{4\pi} = \frac{r_{\rm sph}^2}{4\, r_{\rm BH}^2}, \quad (11)$$

$$r_{\rm sph} = \left(\frac{m_{\rm sph}}{\frac{4\pi}{3} \langle \rho \rangle} \right)^{1/3}, \quad (12)$$

where $m_{\rm sph}$ is the mass of the SPH particle, $r_{\rm sph}$ is the effective size of the particle and $r_{\rm BH}$ is the distance to the BH. The "area filling factor" ($\epsilon_{\rm A}$) and volume filling factor ($\epsilon_{\rm V}$) are the fractions of the SPH particle's area and volume covered by the cold clouds, respectively:

$$\epsilon_{\rm A} = \epsilon_{\rm V}^{2/3}\, N_{\rm cl}^{1/3}, \tag{13}$$

$$\epsilon_{\rm V} = f_{\rm cold}\, \frac{\rho_{\rm sph}}{\rho_{\rm cl}}, \tag{14}$$

where $N_{\rm cl} = f_{\rm cold}\, m_{\rm sph}/m_{\rm cl}$ is the number of clouds within the particle. In this formulation, $m_{\rm cl}$ is a free parameter that serves mainly to set the surface area to volume ratio of the NL clouds. We assume that each cloud has a constant mass $m_{\rm cl} = 200 M_{\odot}$, which yields NLR sizes of $\sim$ 100 pc - 1 kpc, in rough agreement with observed NLRs.

The fractional solid angle subtended by the clouds in each particle is then

$$f_{\Omega} = \frac{\epsilon_{\rm A}\, \Omega_{\rm sph}}{4\pi}. \tag{15}$$

In order to avoid allowing a photon to be absorbed by multiple clouds, we truncate the NLR beyond the radius where the total covering fraction of clouds reaches unity. While this method is not exact, it does allow for the correct rate of ionization in an average sense.

2.3.5 *Selection criteria for ionization parameter & density*

For the remaining gas particles, we calculate the ionization parameter for the cold clouds in a given SPH particle when ionized by a single BH:

$$U = \frac{Q}{4\pi r_{\rm BH}^2 c\, n_{\rm H,cl}}, \tag{16}$$

where $n_{\rm H,cl} = \rho_{\rm cl}/\mu m_{\rm H}$ is the number density of the NL clouds and $r_{\rm BH}$ is the distance from the BH to the cloud. The ionization parameter quantifies the ratio of the ionizing photon density to the electron density at each cloud. In the case of a galaxy merger where two active BHs may be present, the ionization parameter becomes

$$U = \frac{1}{4\pi c\, n_{\rm H,cl}} \left(\frac{Q_1}{r_{\rm BH1}^2} + \frac{Q_2}{r_{\rm BH2}^2} \right), \tag{17}$$

where the subscripts "1" and "2" refer to the primary and secondary BHs. We select only particles with U in the range $10^{-4.5} - 10^{-1.5}$, based on results from photoionization models of NL regions (cf. Osterbrock & Ferland 2006).

Finally, we must ensure that the cloud densities themselves are reasonable. We therefore impose an additional cut on the SPH particles such that only those with $n_{\rm H,cl}$ in the range $10^2 - 10^6$ cm^{-3} are included. The maximum density is typically the more limiting criterion, and is chosen to be roughly equal to the critical density for [O III] emission. Above this density, collisional de-excitation begins to dominate over the forbidden-line emission. While we do not consider forbidden lines in our model, we know they are present in real NLRs, and further that AGN typically have [O III]/H$\beta \gtrsim 3$. Thus, gas above the maximum density will not contribute to the NL AGN profile in a conventional manner, and we exclude these particles from our NL model.

2.3.6 *Identification of gas particles with each BH*

After the galaxies have undergone a close passage, and especially during their final coalescence, particles are easily exchanged between galaxies, and the initial identifications of which particles are in which galaxy are no longer relevant. Thus, we need criteria for assigning particles to each BH at any point in the simulation. When the galaxies are near coalescence, the identification of an SPH particle with one galaxy or the other is less physically meaningful, but it is still helpful for understanding the merger kinematics. Because we are concerned primarily with the relationship of gas particles to the central BHs, we assign particles to each galaxy based on their proximity to and degree of photoionization from each BH. Specifically, we switch gas particles from their initial galaxy identification if a) they are closer to the BH in the other galaxy and b) the quantity $Q/r_{\rm BH}^2$ is 4 times larger for the BH in the other galaxy (i.e., $U_{1,2}/U_{2,1} > 4$).

2.4 Hβ Luminosity and Velocity Profiles

2.4.1 *Hβ luminosity*

Once we have selected SPH particles with cold-phase gas in the desired ranges of U and $n_{\rm H}$ that we believe should contain narrow-line emitting clouds, we may estimate the Hβ luminosity of each cloud, $L_{\rm H\beta}$. While [O III] is generally the strongest narrow emission line, and thus has been the focus of most searches for dNL AGN, for our models the Hβ line offers the advantage that its recombination coefficient depends only weakly on temperature, and thus the line strength is much less sensitive to the exact conditions in the ISM. We note that our use of the Hβ line means that our results for the lifetime of observable NL emission should be considered lower limits. $L_{\rm H\beta}$ may be written as

$$L_{\rm H\beta} = h\, \nu_{\rm H\beta}\, \frac{\alpha_{\rm H\beta}^{\rm eff}(T)}{\alpha_{\rm B}^{\rm eff}(T)}\, f_{\Omega}\, Q\,, \tag{18}$$

where Q is the rate of ionizing photon production as before, f_{Ω} is the cloud covering fraction discussed above, and $\alpha_{\rm H\beta}^{\rm eff}(T)/\alpha_{\rm B}^{\rm eff}(T) \approx 1/8.5$ is the number of Hβ photons produced per hydrogen recombination for $T = 10^4$ K (Osterbrock & Ferland 2006). Thus, when two ionizing sources (two BHs) are present, the total Hβ luminosity is

$$L_{\rm H\beta} = \frac{h\, \nu_{\rm H\beta}}{8.5}\, \frac{\epsilon_{\rm A}}{4\pi}\, (\Omega_{1,\rm sph}\, Q_1 + \Omega_{2,\rm sph}\, Q_2)\,. \tag{19}$$

2.4.2 *Hβ velocity profiles*

In order to understand the kinematics of the NLR as they relate to observations, we construct and analyze velocity profiles for each NLR. From the simulations we have the 3-D velocities for each NL-emitting SPH particle, measured with respect to the stellar center of mass. After projecting these along a given sight line, we assume that within each particle, the NL clouds have a Gaussian internal velocity dispersion with a full-width at half maximum (FWHM) equal to 0.5 $c_{\rm sound}$. The resulting total velocity profile is then convolved with a Gaussian to degrade it to the desired resolution, chosen to correspond to the spectral resolution of SDSS or DEIMOS at typical redshifts for dNL AGN (we use a fiducial value of 65 km s^{-1}).

3 RESULTS

3.1 Evolution of Narrow-Line AGN in Major Mergers

3.1.1 General Properties

The maximum BH separation for which double NLs could result from BH motion is set by the size of the spectral slit or fiber of the instrument taking the observations. The size of the spectral slit on the DEIMOS spectrograph is 0.75", corresponding to 5.36 kpc at $z = 0.7$. Thus, only a binary BH with separation $a_{\rm max} \lesssim 5.36$ kpc could be observed to have double NLs with DEIMOS. The diameter of the SDSS spectroscopic fiber is 3", which projects to 5.47 kpc and 21.4 kpc at $z = 0.1$ & 0.7, respectively. Thus, for the mean redshifts of each sample, the dNL AGN diagnostic is sensitive to binaries with projected separation $\lesssim 5.5$ kpc.

For our analysis of NLRs in galaxy merger simulations, we divide the merger evolution into phases based on these limits for observing double NLs, considering both a maximum BH separation of $a_{\rm max} = 5.5$ kpc, corresponding to systems at $z \sim 0.1$, and a larger value $a_{\rm max} = 21$ kpc, corresponding to higher-redshift systems. We refer to the early merger stage as Phase I, when the NLRs are well-separated and could not be observed in a single spectrum ($a_{\rm sep} > a_{\rm max}$). Phase II we refer to as the "kiloparsec-scale phase", which occurs when the following criteria are met: (i) $a_{\rm sep} < a_{\rm max}$, (ii) at least one BH has an active NLR, and (iii) the BHs have not yet merged. We define the post-BH-merger phase as Phase III. If for any period between Phases I & III the Phase II criteria (i) & (ii) are not met, we define this period as Phase IIb.

In Fig. 1, we show the evolution of AGN activity and the NLRs throughout a major merger. The Hβ luminosity traces the bolometric luminosity; both curves have (Eddington-limited) peaks after the first pericentric passage of the two galaxies and a larger peak during the final coalescence. Note, however, that the NLR is not active at all for the first 600 Myr of the merger simulation, owing to the low BH luminosity. Only after the galaxies undergo a close pericentric passage is the BH luminosity high enough for the gas particles to meet our minimum criteria for an active NLR. At the end of the simulation, 200 Myr after the BH merger, $L_{\rm bol}$ and $L_{\rm H\beta}$ have passed their peaks and begun to decline. Note that the two NLRs have comparable Hβ luminosities, within a factor of ten, throughout most of the simulation (as do the two AGN), though they differ by about two orders of magnitude for short periods of time. We do not require that the total Hβ luminosities from each NLR be comparable in order to produce dNLs, or even that both NLRs be active. In practice, we find that dNL AGN usually occur when both NLRs are active, though their Hβ luminosities may differ substantially.

Fig. 1 also demonstrates a key feature of AGN triggered by major, gaseous mergers: peak AGN and NL activity typically occurs during the final coalescence of the two galaxies. Under the assumption of efficient BH mergers, this means that peak activity also roughly coincides with the BH coalescence. This has important implications for the observability of dual AGN. In essence, merger-triggered AGN are typically brightest both shortly after the BHs have merged and during the kiloparsec-scale phase of BH inspiral. § 3.4 illustrates that this simple fact enhances the probability of observing dNL AGN in the kpc-scale phase versus earlier stages in the merger.

Another notable feature in Fig. 1 is the small gap and dip in $L_{\rm H\beta}$ that occur near the time of BH merger and peak $L_{\rm bol}$. This is also when the central gas density in the merger remnant reaches its peak, and for a brief time the gas densities surrounding the BHs exceed our maximum density criterion for NLR particles. As described in § 2.3.5, in such conditions the emission from collisional de-excitation begins to outweigh forbidden-line emission, so this gas cannot be considered part of the narrow-line region as it is typically defined for an AGN (with, e.g., [O III]/H$\beta \gtrsim 3$). This gap in NL emission occurs only in the mergers that attain the highest peak densities, i.e., those with nearly equal mass and moderate-to-high gas fractions. Without arbitrarily high-resolution simulations or radiative transfer calculations, it is difficult for us to say exactly what the emission from this region would look like in reality at these moments of peak density. However, it seems plausible that even if a decrement in luminosity does not occur for permitted lines such as Hβ, this could occur for forbidden lines such as [O III] when the gas density exceeds their critical densities. In any case, because these gaps in emission are brief, they do not affect our results qualitatively and have only a small effect on our quantitative results. Specifically, the dNL AGN lifetimes increase by $< 50\%$ for $n_{\rm max}$

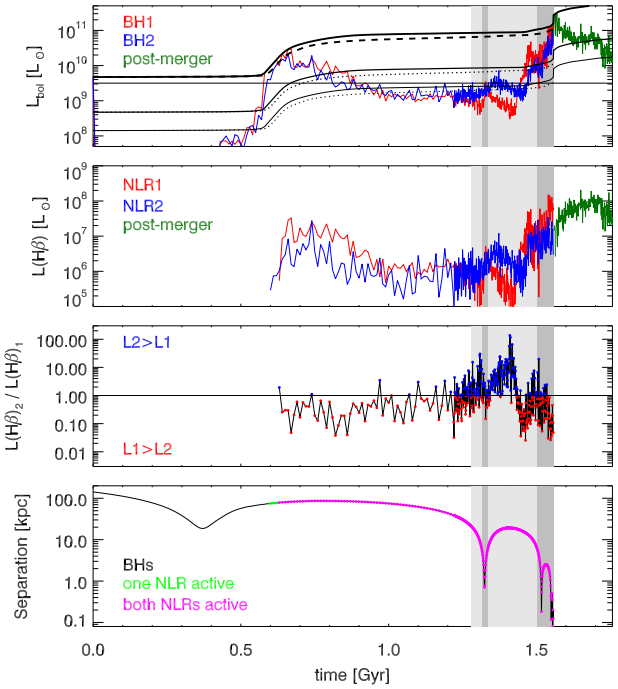

Figure 1. Time evolution of relevant quantities for an equal-mass merger containing 10% gas initially. In each panel, the gray-shaded regions denote Phase II, i.e., the kpc-scale phase. The dark-gray shade denotes BH separations of < 5.5 kpc, which corresponds to the size of the SDSS spectroscopic fiber for objects at $z \sim 0.1$, or the size of the DEIMOS spectral slit for objects at $z \sim 0.7$. The light-gray shade denotes BH separations of < 21 kpc, corresponding to the size of the SDSS fiber for objects at $z \sim 0.7$. Top plot: bolometric luminosity ($L_{\rm bol}$) versus time. Blue and red curves denote each BH's luminosity prior to the BH merger, and the green curve denotes $L_{\rm bol}$ after the merger. The thick solid and dashed lines (uppermost) denote the Eddington limit for each BH, and the thin solid and dotted lines denote three different definitions of an AGN (3% & 10% $L_{\rm Edd}$ for each BH, and a constant-luminosity definition of 3×10^9 L$_\odot$). Upper-middle plot: Hβ luminosity (L(Hβ)). Same color scheme as in top plot. Lower-middle plot: Ratio of $L_{\rm H\beta}$ for each BH. Points where $L_{\rm H\beta 2} > L_{\rm H\beta 1}$ are shown in blue, and those where $L_{\rm H\beta 1} > L_{\rm H\beta 2}$ are shown in red. Bottom plot: BH separation vs time. The magenta points denote the NLR center-of-mass separation versus time for the snapshots in which both NLRs are simultaneously active.

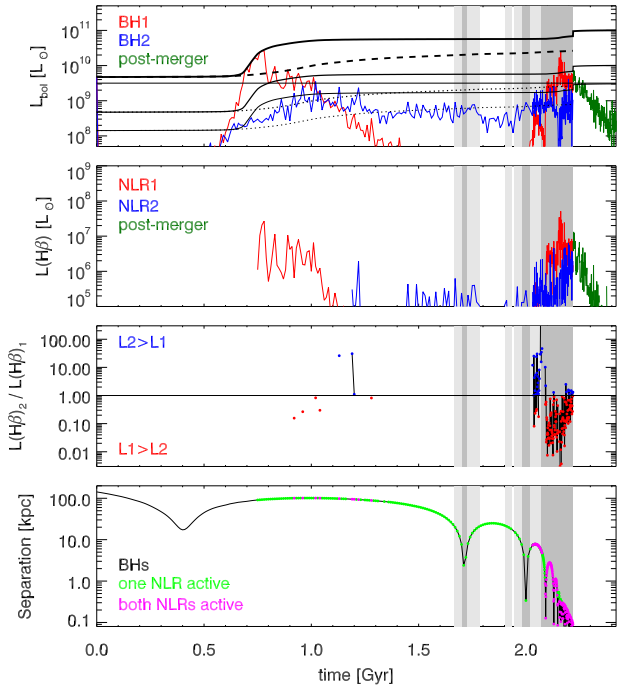

Figure 2. Same quantities as in Fig. 1, but for a merger model with a mass ratio $q = 0.5$ and initial gas fraction $f_{\rm gas} = 0.04$.

as high as 10^8 cm^{-3}—much less than the variation in these lifetimes for different viewing angles, which is often an order of magnitude or more (see § 3.4 for further discussion of dNL AGN lifetimes).

The total merger time from the start of the simulation to the time of BH merger is 1.6 Gyr, but Phase II, shaded in dark and light gray for $a_{\rm max} = 5.5$ and 21 kpc, respectively, has a duration of 72-278 Myr. In general we find that the BHs, and their NLRs, evolve fairly rapidly to small separations once they enter the kpc-scale phase during the final coalescence of the two galaxies. This is a consequence of efficient dynamical friction and gas drag in the dense merger remnant potential, and it ensures that Phase II is always a small fraction of the total merger timescale.

Our progenitor galaxies initially have 4 - 30% of their baryonic mass in gas. This gas is depleted substantially via star formation during the course of the merger; at the onset of Phase II, the gas content is typically about half of its initial value. However, major mergers are efficient at rapidly fueling gas to the central regions of galaxies, such that by this point in the merger the remaining gas, as well as the newly-formed stars, dominate the central region of each merging galaxy.

3.1.2 Dependence on Merging Galaxy Parameters

We find that the amount of NL activity in a galaxy merger is strongly influenced by the mass ratio and gas content of the host galaxies. Fig. 2 shows the same quantities as Fig. 1, but for an unequal-mass merger ($q = 0.5$) with a low initial gas fraction of $f_{\rm gas} = 0.04$. The BH in the primary galaxy has an Eddington-limited burst of accretion following the first close passage, triggering strong feedback that heats the surrounding gas and limits further accretion until final coalescence. The secondary BH never reaches its Eddington limit but maintains a fairly constant $L_{\rm bol}$ following the pericentric passage until final coalescence. While at least one of the NLRs is active for most of the simulation, they are simultaneously active virtually only during the kpc-scale phase, and even then the $L_{H\beta}$ ratio fluctuates significantly. Notably, in this example the peak of AGN and NL activity occurs several tens of Myr prior to the BH merger, and thus most of the NL activity coincides with the kpc-scale phase. In contrast, the peak $L_{\rm bol}$ in example in Fig. 1 is nearly simultaneous with the BH merger. Nonetheless, we see that substantially less NL activity occurs in this low-$f_{\rm gas}$, unequal-mass merger than in the previous example. This holds true of our merger models in general; mergers with lower mass ratios and gas fractions have less AGN and NL activity, and thus are less likely to produce observable dNL AGN. (See § 3.4 for a comparison of dNL lifetimes.) This is as expected, because equal-mass mergers induce the strongest perturbations in the merging galaxies, causing more gas to lose angular momentum and flow rapidly to the galaxy centers. Galaxies with substantial gas reservoirs will likewise provide more fuel to the central BHs than those that are gas-poor. However, two additional effects, described below, cause the NL activity in Phases II and III to be especially sensitive to the merging galaxy parameters.

As mentioned in § 3.1.1, the peak BH accretion rates for major, gaseous mergers are generally higher during final coalescence than following the first close passage. This owes in large part to the fact that the BH masses, which are initially quite small, are typically 1 - 2 orders of magnitude larger at coalescence than at the first passage. Thus, their Eddington limits are larger by the same factor. (The Bondi accretion rates are proportional to the mass squared, but of course depend heavily on environment as well.) In most of our simulations, the BHs experience Eddington-limited bursts of accretion following the first passage and at coalescence, as in the example in Fig. 1. However, in mergers with lower q and $f_{\rm gas}$ the BHs may not reach the Eddington limit, or accretion and feedback early in the merger may deplete much of the central gas reservoir. In these cases, including the example in Fig. 2, the AGN luminosity may actually be *lower* during coalescence than after the first passage. Therefore, such mergers have relatively low-level NL activity and contribute little to the population of dNL AGN. Note that this supports the argument in § 3.1.1 that most merger-triggered dNL AGN that are *observable* should be found in the late stages of merging, i.e. in Phases II and III.

A related effect is that in nearly-equal-mass, gaseous mergers, the rapid inflow of gas that fuels the peak BH accretion during final coalescence of the galaxies can also cause rapid changes to the central potential of the merger remnant. Specifically, the central escape speed ($v_{\rm esc}$) may increase substantially between the kpc-scale phase and the post-BH-merger phase. As the central potential deepens, the BH and gas velocities increase. This causes longer-lived and more-pronounced double-peaked NLs via BH motion and via gas rotation. In such cases, the fraction of double-peaked NLs associated with dual versus single AGN depends on the timing of the BH inspiral and merger relative to the increase in central $v_{\rm esc}$. This is the same effect noted by Blecha et al. (2011) in the context of its importance for the timing of gravitational-wave (GW) recoil kicks. By assuming that the BHs merge efficiently (i.e. within one timestep when $a_{\rm sep} < r_{\rm soft}$ and $v_{\rm rel} < 0.5\,c_{\rm sound}$), we find that this effect leads to a larger fraction of Phase III (post-BH-merger) dNL AGN. This is discussed further in § 3.3.3 & 3.4. However, this increase in $v_{\rm esc}$ occurs only for nearly-equal-mass, relatively gas-rich mergers. For the merger models presented here, only those with $f_{\rm gas} = 0.3$ show a noticeable $v_{\rm esc}$ increase at coalescence, and

only in the $q = 1$, $f_{\rm gas} = 0.3$ model does $v_{\rm esc}$ increase by more than ~ 200 km s^{-1}.

We note that the same processes that fuel AGN can also trigger rapid star formation, which may produce large amounts of dust that could obscure activity in the central region. The problem is especially complex for the NLR, which exists at large enough radii to be intermingled with the newly-forming central cusp of stars. Because the present work, as a first attempt to model the NLR in galaxy mergers, does not account for the potential effects of dust obscuration, we must consider this an important caveat to interpretations of our simulated NLRs as "observable". In order to avoid as much as possible a strong-starburst regime, we do not consider initial gas fractions above 30%, and much of the analysis presented here concerns galaxies with $f_{\rm gas} \leq 0.1$ initially. Thus, our simulations produce low- to moderate-luminosity AGN, rather than luminous quasars. Furthermore, while the peak SFR following the first pericentric passage can be in excess of 100 M$_\odot$ yr^{-1} for our higher-q and $f_{\rm gas}$ simulations, the peak SFR during final coalescence (i.e., during Phase II) is typically much lower, $\lesssim 1 - 10$ M$_\odot$ yr^{-1} for these same simulations. For lower-q, $f_{\rm gas}$ mergers, the peak SFR is much lower than this; the example in Fig. 2 has a peak SFR at coalescence of only 0.4 M$_\odot$ yr^{-1}.

We also consider the addition of a stellar bulge component to our progenitor galaxies, which are nominally pure disks in these simulations. It is well-known that the presence of a bulge can act to stabilize a galactic disk to perturbations during encounters, thereby delaying catastrophic loss of gas angular momentum until the final coalescence of the galaxies (e.g., Mihos & Hernquist 1996). Much of the star formation and BH growth triggered by gas inflow is thereby similarly delayed. We consider bulges containing 10 - 20% of the total stellar mass, and find that the SFR and BH accretion rate are lower following the first passage and are slightly higher during coalescence. The effect is stronger for the SFR and for higher $f_{\rm gas}$; the peak SFR can change by a factor of several in each direction. However, because AGN and NL activity is generally highest during coalescence in any case for the mergers that produce the most AGN activity overall, the presence of a bulge only enhances this effect.

The multiphase ISM model of Springel & Hernquist (2003) includes a parameter, $q_{\rm EOS}$, that determines the degree of "softening" of the gas equation of state (EOS); when this parameter is set to zero, the EOS is purely isothermal, and when it is set to one, the full multiphase ISM model is used. Intermediate values of $q_{\rm EOS}$ interpolate between these two. We adopt a fiducial value of $q_{\rm EOS} = 0.25$, as in Springel & Hernquist (2003), but because of the potential for the choice of EOS to affect our results, we also test values of 0.5 and 0.05 for select merger models. In general, the gas disk is more stable for the softer EOS ($q_{\rm EOS}$ = 0.5), and it is much more prone to fragmentation and has a very clumpy distribution for $q_{\rm EOS} = 0.05$. This causes higher accretion rates in the latter case, including sustained higher accretion rates following the first close passage of the two galaxies. The final BH masses may be up to an order of magnitude higher for $q_{\rm EOS} = 0.05$ versus 0.5, and the dNL AGN lifetimes may be larger by a similar factor in Phases II & III. In the early merger phase (Phase I), the disparity may be even greater, as Phase I dNL AGN lifetimes are generally quite low for the softer equations of state. (See § 3.4 for more discussion of dNL lifetimes.) The simulations with $q_{\rm EOS} = 0.5$ are more similar to those with our fiducial value than with $q_{\rm EOS} = 0.05$, but they do have less NL activity. We consider the nearly-isothermal EOS ($q_{\rm EOS} = 0.05$) to be a fairly extreme model, but regardless we note that the BH activity in these mergers does depend to some degree on the gas EOS. Specifically, gas distributions that are clumpier and closer to isothermal should result in more AGN and NL activity.

Finally, we have examined the dependence of our results on the mass and spatial resolution of the simulations, using a set of simulations of the $q = 0.5$, $f_{\rm gas} = 0.1$ merger model. We test baryonic mass resolutions of a factor of two higher and lower than our fiducial value, and we test DM resolutions up to a factor of five higher than our fiducial value. The gravitational softening lengths are accordingly scaled $\propto M^{1/3}$. We find that our results are broadly quite similar for all of these simulations. There is a trend toward somewhat higher central densities for higher resolutions; this essentially reflects the need for the multiplicative factor for the accretion rate, described in § 2.1, which accounts for the higher densities not captured on sub-resolution scales. Owing to the approximate nature of the sub-resolution BH accretion model, it is impossible to know the "true" value to which the accretion rates should converge, and this must be considered a source of uncertainty in any numerical study utilizing semi-analytic BH models, including the present work. However, the dependence of central density and corresponding accretion rate on resolution is weak; in our resolution study the peak bolometric and Hβ luminosities vary by at most a factor of a few over the resolutions sampled, and the *integrated* BH accretion rates (i.e., the final BH masses) are very nearly identical. Also, the lifetimes of double-peaked NL AGN in these simulations, when averaged over many random sight lines, have less variation with resolution than with the observer's line of sight.

3.2 NLR Morphology

Here we examine in detail the size, structure, and Hβ luminosity of the NLRs. Fig. 3 shows velocity maps of the NLRs at various stages of the merger, along with corresponding $L_{\rm H\beta}$ maps. The first pair of plots shows a snapshot about 150 Myr after the onset of NL activity following the first close passage of the galaxies. We see that each NLR is $\gtrsim 500$ pc across, has a disky structure as seen in the xz projection, and is in rotation. Additionally, in the first galaxy (left panels in each plot), a gap in the NLR is seen in the disk midplane. Because the gas density is highest along the midplane, some of them may exceed our maximum-density criterion as described above. The next pair of plots (top right) shows a snapshot later in the merger, when $L_{\rm bol}$, $L_{\rm H\beta}$, and the gas density are near their minima between the first passage and final coalescence of the galaxies. Accordingly, the NLRs are fainter and more diffuse and extended. Note that the same disk-like structure is still apparent. In the following snapshot (middle-left pair of plots), the NLRs are shown just after a pericentric passage ~ 200 Myr prior to BH merger; the BH separation here is 0.76 kpc and thus the merger is well into Phase II. Unlike the first two snapshots shown, the BHs show strong relative motion apparent in all three projections, and the corresponding relative motion of the NLRs is especially apparent in the xz projection. The NLRs are still quite diffuse and faint here, with $L_{\rm H\beta} \sim$ few $\times 10^6$ L$_\odot$.

Soon thereafter, as the galaxies near their final coalescence, the rapid inflow of gas increases the central gas density. As the next snapshot (middle-right pair of plots) shows, the NLRs become denser, brighter, and more compact. Their shape becomes more spherical, as their size is now limited by the self-shielding criterion described in § 2.3.4, but a preferred axis for the brightest Hβ emission can still be seen, especially in the xz and xy projections. Strong rotation features are also still apparent, though overall blue- and redshifts are also seen in the xz projection for each galaxy, respectively, owing to their relative motion. The latter feature is

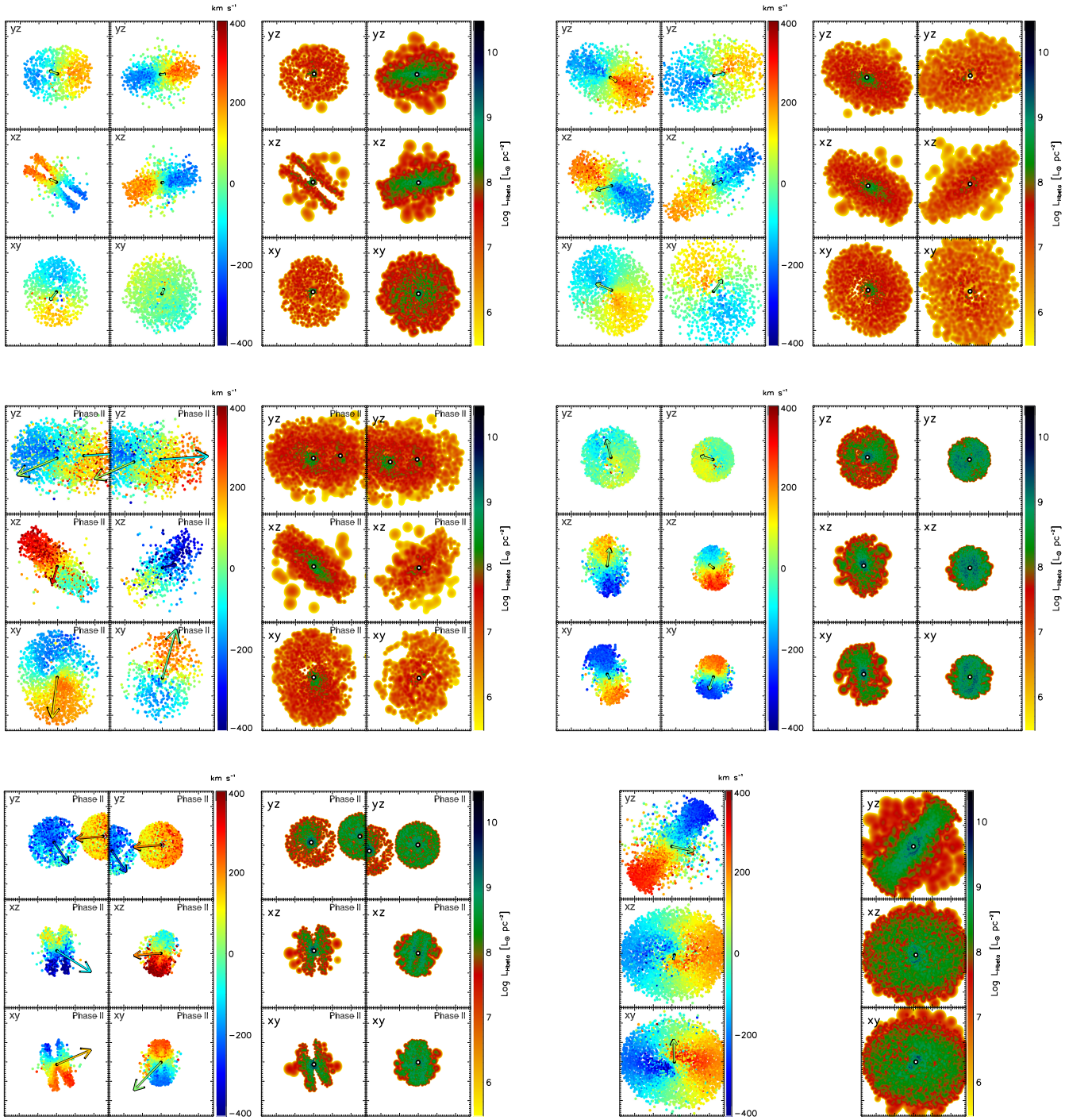

Figure 3. LOS velocity maps and $L_{\mathrm{H}\beta}$ maps of NLRs at six different snapshots throughout a single galaxy merger. In each pair of plots, the left plot is the velocity map and the right plot is the $L_{\mathrm{H}\beta}$ map. In each 6-panel plot, the left column of shows three orthogonal projections centered on BH2, and the right column shows the same three projections centered on BH1. The final pair of plots is a post-BH-merger snapshot, so only one column of panels is shown. In the velocity maps, the magnitude of the colored arrows denotes the projected BH velocity, and their hue denotes the LOS BH velocity. Each panel is 800 pc on a side, and the velocity scale spans from -400 km s^{-1} (red) to +400 km s^{-1} (blue). This sign convention for LOS velocity is used throughout the paper. The panels in the $L_{\mathrm{H}\beta}$ maps are also 800 pc on a side.

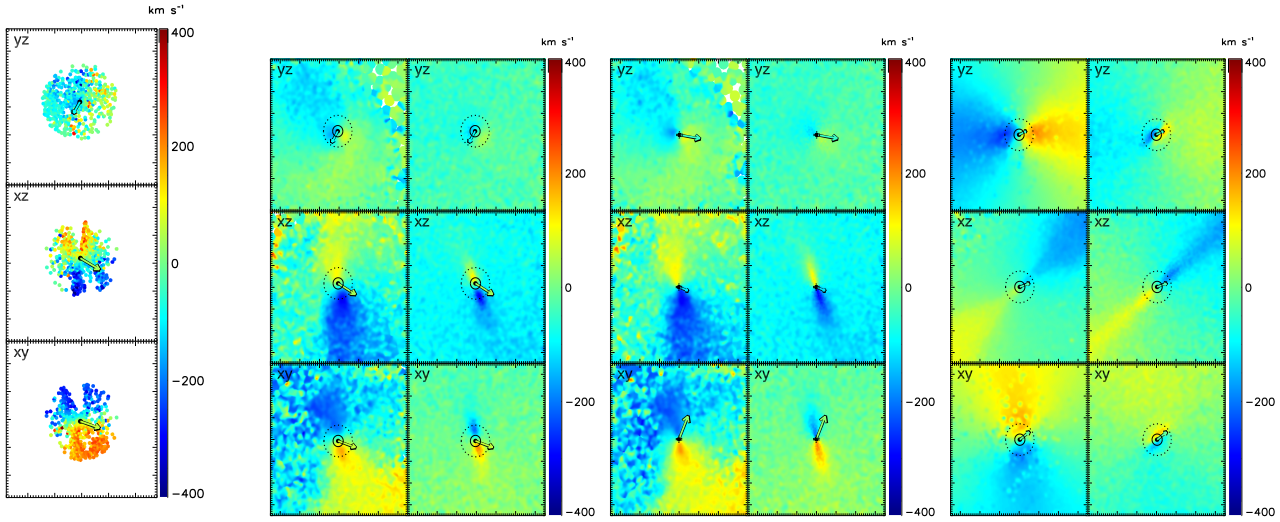

Figure 4. Left plot: Hβ velocity map centered on one BH, in three projections, in a similar manner as in Fig. 3. The BH velocity vectors are also plotted here as in Fig. 3. The simulation shown has $q = 1$ and $f_{\rm gas} = 0.1$ initially. **Left-middle plot:** For the same simulation, the velocity map is shown for the *total* gas distribution (rather than only the NL gas) in the left panels, and for the total *stellar* distribution in the right panels. The solid circle drawn around the BH denotes the gravitational softening radius ($r_{\rm soft}$), and the dashed circle denotes $2.8r_{\rm soft}$, the point at which the gravitational force becomes fully Newtonian. **Right-middle plot**: The same gas and stellar velocity maps are shown as in the previous plot, for the same merger model, but with the merger partially re-simulated with an $r_{\rm soft}$ that is 5 times smaller. The same circles are drawn here, but because $r_{\rm soft}$ is smaller, their size barely exceeds that of the dot that marks the BH position. **Right plot**: The same gas and stellar velocity maps are shown, but for a different merger model with $q = 1$ and $f_{\rm gas} = 0.3$. The larger gas supply causes enhanced central star formation and a kinematic feature extending well beyond $r_{\rm soft}$.

greatly magnified in the next snapshot (lower-left plots), occurring just before a close passage of the BHs, 42 Myr prior to their merger. As in the previous close-passage snapshot, strong relative motion is apparent in all three projections, but here $L_{\rm bol}$ and $L_{\rm H\beta}$ are about 10 times higher. This is in fact an example of a double-peaked NL AGN induced by BH motion, as will be discussed in the next section. Finally, the last two plots (lower-right) show the final snapshot of the simulation, 200 Myr after the BH merger. The gas density, $L_{\rm bol}$ and $L_{\rm H\beta}$ have all declined, causing the NLR to again become more diffuse, but still with higher density and Hβ luminosity than in the early-merger phase.

The persistence of flattened, rotating NLR morphologies throughout the merger is critical for the resulting velocity profiles; many double-peaked profiles arise simply from the rotation of these disk features, rather than from the relative BH motion. As such, these features merit closer examination. If we define the BH radius of influence as the radius at which the baryonic mass surrounding the BH equals twice its mass ($r_{\rm infl} \equiv r(M_{\rm b} = 2M_{\rm BH})$), then $r_{\rm infl}$ ranges from $\gtrsim 100$ pc early in the merger, when the gas density is low, to only a few pc at late stages when the gas density is much higher. Thus, at all times, $r_{\rm NLR} \gg r_{\rm infl}$, so the gravitational potential of the BH alone is not responsible for keeping the NL clouds bound in coherent rotation. However, following the first close passage of the galaxies, a dense cusp of new stars begins to form in the central region of each galaxy. As was discussed in § 3.1.1, this stellar component is dominant within the central $\sim$ kpc. Fig. 4 demonstrates that the kinematics of the NL gas matches that of the central gas distribution, which itself traces the kinematics of the stellar cusp. Therefore, we see that it is indeed the gravitational potential of the newly-formed stars, as well as their angular momentum, that creates the flattened rotation features in the NLRs seen in Fig. 3.

A remaining question is whether the softened gravitational potential used in our simulations has a nonnegligible effect on the kinematic structure of the central region. The gravitational softening length used in our simulations is $r_{\rm soft} = 37$ pc, which is smaller than the size of our NLRs, but because of the softening kernel used, the gravitational forces are not strictly Newtonian until $2.8r_{\rm soft}$, i.e., 104 pc. When the galaxies are near coalescence and the NLRs are most compact, their size can indeed be comparable to this value. We have drawn these two radii, $r_{\rm soft}$ and $2.8r_{\rm soft}$, on the panels in Fig. 4. In the first example, the central stellar rotation feature is comparable in size to the extent of the softening kernel. However, we have resimulated part of this merger with a softening length five times smaller, and we show the result for the same snapshot in the second plot. Here, the circle drawn at $2.8r_{\rm soft}$ is barely larger than the size of the dot used to denote the BH position, yet the kinematic stellar structure has the same spatial extent. In fact, the smaller softening length seems to allow the stellar rotation to persist down to smaller scales around the BH. This is evidence that if anything, the gravitational softening "washes out" rotation features on scales of < 10 pc, and certainly is not artificially inducing or supporting rotation on larger scales. In both cases the motion of the gas traces that of the stars, so we can have similar confidence in the rotation observed in our NLRs. Additionally, we find that the central, rotating cusp of stars does not appear until after the first burst of star formation following the close passage of the galaxies; prior to this, the velocity map is featureless in this central region. This supports the picture in which a newly-formed cusp of stars supports the rotation seen in the NLRs, and argues against a numerical origin since the gravitational softening remains constant throughout the simulation. Further evidence along these lines comes from the third plot in Fig. 4, which shows a snapshot from an equal-mass merger with a higher gas fraction ($f_{\rm gas} = 0.3$). In this simulation, the higher gas content provides more fuel to the central regions for star formation, and accordingly a much more extended, disk-like rotating stellar feature can be seen in the velocity map, well beyond $2.8r_{\rm soft}$. The

softening length remains the same in this simulation, so the larger spatial extent of the coherent rotation in this example must result from the larger gas content of the galaxies.

3.3 Observable Signatures of kpc-scale Double-NL AGN

3.3.1 NLR Kinematics

In Figs. 5 - 7, we illustrate some examples of kiloparsec-scale dual AGN with double-peaked NLs, looking in detail at their kinematic features. Foremost, these examples demonstrate that a variety of velocity structures can give rise to dNL AGN during the kiloparsec-scale phase. Fig. 5 (the yz projection; top panels) is an example of the "standard" picture that motivates the association of dNL AGN with dual BHs. We see two distinct NLRs, one associated with each BH, with NLR LOS velocities corresponding to the substantial LOS velocities of the BHs. The velocity profile (v_x; first column) shows a bright, slightly blueshifted peak arising from the NLR associated with "galaxy 1", and a fainter, highly redshifted peak arising from the other NLR. The combined profile, which is what an observer would see, is a double-peaked NL with peaks almost perfectly aligned with the BH velocities and a peak separation of ~ 300 km s^{-1}. This is an example of a dNL AGN resulting directly from BH motion, at a time when the NLRs are still distinct and non-overlapping (the BH separation is 0.79 kpc).

Fig. 6 also shows a dNL AGN that results directly from BH motion, but in a very different regime. Here, the BH separation is comparable to the size of the NLR, so we would not expect two distinct density peaks to be resolvable in the stellar image. In this particular case, the luminosities of the two BHs are quite different; we see in the middle panels of the velocity profile that the BH associated with galaxy 2 is much fainter. As a consequence, the NLR emission arises almost entirely from ionization by the first BH. However, it is obvious from the velocity map that the second BH is influencing the NLR kinematics as it nearly plows through the NLR. Note that the resulting double-peaked profile is apparent in all three orthogonal projections, owing partly to the rapid relative motion of the two BHs. This is therefore a second example of a dNL resulting directly from BH motion, but at a later stage in the merger evolution when only a single, common NLR remains. We emphasize that in this example, a dNL AGN results directly from BH motion even though the BHs do not have comparable luminosities. Indeed, because the second BH is interacting with gas that is ionized by the primary BH, the secondary BH need not even be active to produce this type of kinematic feature. Such features will be very short-lived, of course, but should be hard to avoid once the BH separation falls below the size of the NLR, provided there is sufficient motion in the LOS. This is important for the likelihood of observing such systems, as AGN frequently exhibit variability. Furthermore, in other, unequal-mass mergers we find in some cases an additional cause of large differences in AGN luminosity between the two BHs. The smaller BH may be partially stripped of its central cusp of gas and stars as it interacts with the larger stellar cusp during the final inspiral phase (on ~ 100 pc scales). This depletes the reservoir of fuel available to the smaller BH, and thus creates a drop in its accretion rate just prior to merger.

In addition to dNL AGN produced directly by BH motion, we find many examples where double-peaked profiles are produced by gas kinematics but are *influenced* by the BH motion. In other cases, the double-peaked features arising from gas kinematics are simply coincident with the kpc-scale phase; these cases are also of interest, especially as examples of this scenario have already been found in real systems (Fu et al. 2011b). Fig. 7 is an example of the former case, where the BH motion influences a double-peaked profile arising from gas kinematics. The BH and NLR in galaxy 2 has an overall blueshift visible in all three projections, and a single, wide peak. The NLR gas in galaxy 1 is in rotation, such that the BH has a slight redshift but much of the NLR emission (including a second peak in the v_x and v_z projections) is highly redshifted. The combined profile for these projections shows a redshifted, uneven double peak in which the double peak arises from NLR1, but is influenced by the blueshifted peak in NLR2. Thus, the BH motion affects both the centroid and the peak ratio of the combined NLR profile.

It is of great interest, both for future observations and for our theoretical understanding of dual BHs, to estimate the fraction of Phase II dNL AGN in our simulations that are affected either directly or indirectly by the BH motion. Accordingly, we have undertaken a visual analysis of the velocity profiles at each Phase II snapshot, from three orthogonal viewing angles, in two of our simulations (mergers with $q = 1$, $f_{\rm gas}= 0.1$ and with $q = 0.5$, $f_{\rm gas}= 0.3$). We have visually classified each observable double-peaked profile in Phase II as (i) directly induced by BH motion, (ii) indirectly influenced by BH motion, (iii) merely coincident with Phase II, or (iv) a complex or highly asymmetric profile classified as double-peaked by our fitting algorithm. We also consider definitions of Phase II with $a_{\rm max} = 5.5$ & 21 kpc. The fraction of snapshots in each category varies substantially between the three sight lines and two simulations, owing to small number statistics and intrinsic variability with viewing angle and galaxy merger model. Nevertheless, we can draw some general conclusions from this analysis. The directly-induced doubles occur in only a few snapshots, corresponding to lifetimes of 3-6 Myr. These primarily occur for BH separations < 5.5 kpc, and thus can account for up to $\sim 50 - 60\%$ of the Phase II dNL lifetime for the smaller $a_{\rm max}$ definition. If BH separations up to 21 kpc are also considered to be part of Phase II, the fraction of "direct" dNLs drops to between 6 and 33%. Considering instead the total fraction of Phase II for which the BH motion has some influence on the velocity profiles, directly or indirectly, we find this occurs for a majority of Phase II ($a_{\rm max} = 5.5$ kpc), up to 80%, and in the equal-mass model tested, it also occurs for a majority of Phase II with the larger $a_{\rm max}$. Most of the remaining double-peaked profiles arise from gas rotation in a single flattened or disk-like NLR, or from the superposition of two such double-peaked profiles when the BHs have little relative motion. However, in some cases up to 20-30% of the Phase II profiles classified as double peaks are actually complex (multi-peaked) or highly asymmetric profiles. These are important signatures as well, because they are usually also associated with BH motion. The complex profiles, in particular, typically arise either from a highly-disturbed NLR gas distribution following a close passage or from the superposition of two double-peaked profiles with different velocity centroids.

3.3.2 Stellar Structure

In addition to the NLR kinematics, Figs. 5 - 7 also show stellar density maps for each of these examples. In both Fig. 5 and Fig. 7, two density peaks are present in all three projections of the stellar density maps, but would require very high resolution imaging to resolve. In particular, in Fig. 5, the xz projection has the smallest projected separation, despite substantial LOS motion of the BHs. This is a fairly common feature of kpc-scale BH pairs; owing to their rapid inspiral on these scales, their orbits are generally *not*

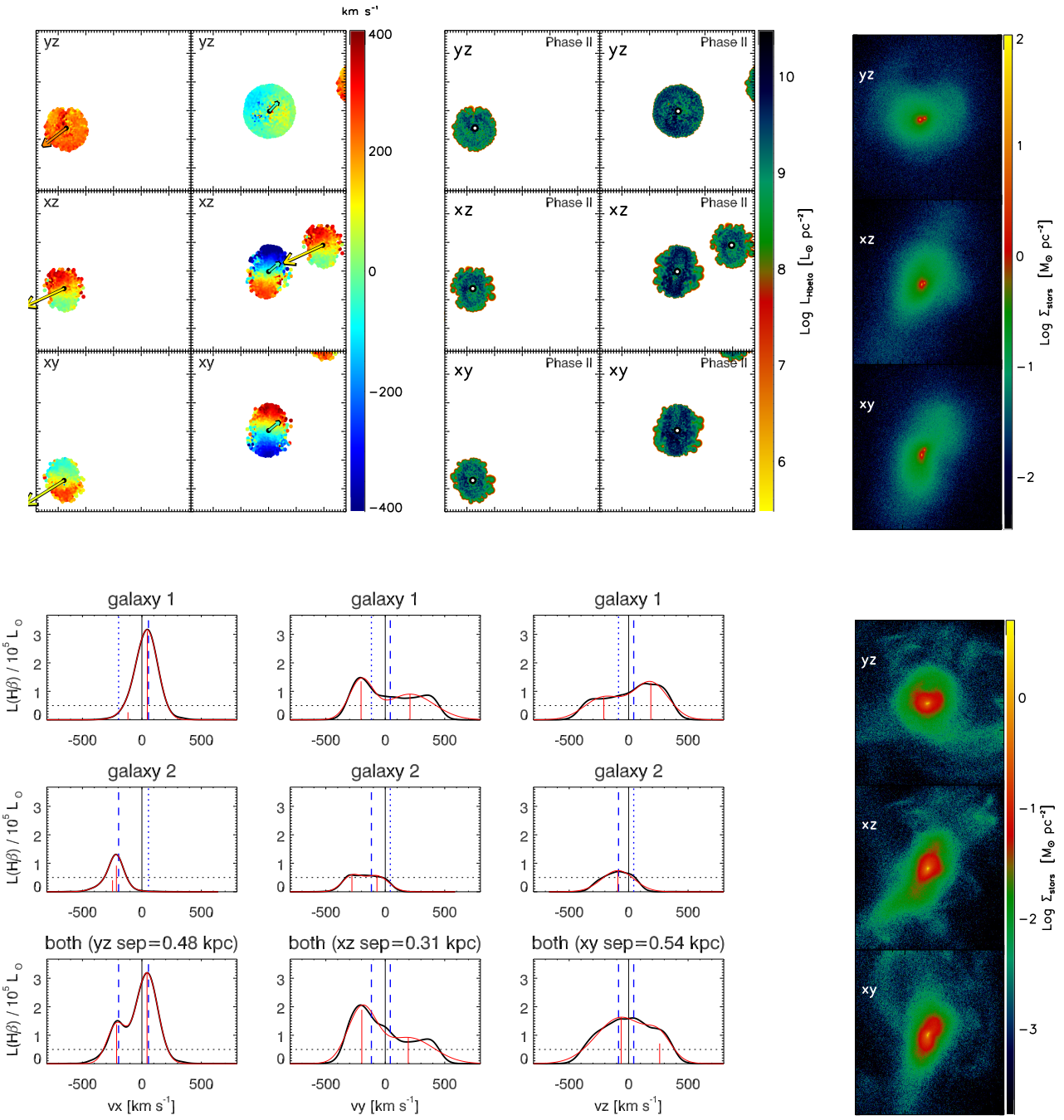

Figure 5. The NLR velocity maps, Hβ luminosity, and 1-D velocity profiles, as well as the stellar density maps, are shown for three orthogonal projections of a single simulation snapshot during the kpc-scale phase (Phase II). The merger model for the simulation shown had $q = 0.5$ and $f_{\rm gas}= 0.3$ initially. The snapshot shown occurs just 8 Myr prior to the BH merger, and the BH separation is 0.79 kpc. **Top left plot**: LOS velocity maps for NLR particles, in the same manner as in Fig. 3. As before, the left column of this plot shows three projections centered on BH2, the right column is centered on BH1, and the arrows denote the BH velocity. **Top middle plot**: map of Hβ surface brightness. The orientation and scale of these panels is the same as in the velocity map (left plot). Here the BH positions are denoted by the black open circle. **Top right plot**: Projected stellar density shown from the same three orientations; each panel is 15 kpc on a side. **Bottom-left plot:** 1-D velocity profiles for the NLRs shown. The three columns show v_x, v_y, & v_z, corresponding to the yz, xz, and xy projections, respectively. The top row shows the profiles for NLR particles associated with galaxy 1 (and BH1), and the middle row shows those associated with galaxy 2 (BH2). The bottom row shows the combined profile. Because this snapshot is within Phase II, the combined profile is by definition what would be seen by observers. In each panel, the black curve shows the profile calculated from simulation data, and the thin red curve is the best fit for a double-Gaussian profile. The horizontal black dotted line marks the minimum threshold we have set for observability of the Hβ line: $L_{\rm H\beta} = 5 \times 10^4$ M$_\odot$. The vertical black line is the rest frame of the host galaxy (stellar center-of-mass velocity), and the blue dashed and dotted vertical lines denote the BH velocities (dashed = BH1 for galaxy 1 and BH2 for galaxy 2) The calculated profiles assume a Gaussian internal velocity dispersion with FWHM $= 0.5c_{\rm sound}$, and are degraded to a resolution of 65 km s^{-1}. **Bottom-right plot:** projected stellar density from three orientations, but on a larger scale than above; each panel is 43 kpc on a side.

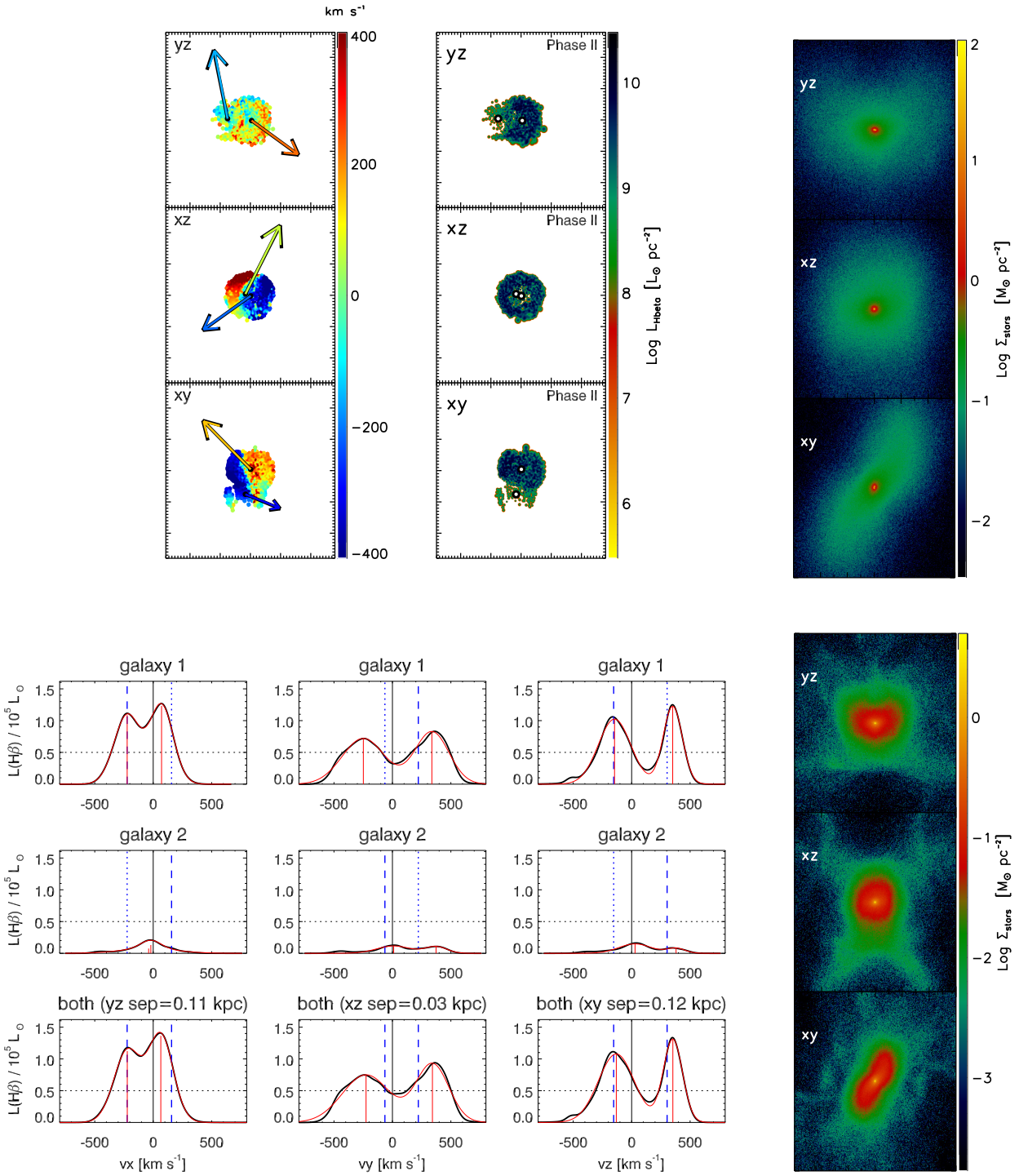

Figure 6. NLR velocity maps, Hβ luminosity maps, and 1-D velocity profiles, as well as stellar density maps, are shown in the same manner as Fig. 5, for a Phase II snapshot in a simulation with $q = 1$ and $f_{\rm gas} = 0.1$ initially. This snapshot also occurs 8 Myr prior to BH merger, but here the BH separation is only 0.17 kpc.

circular. Thus, the largest LOS velocity separation may occur when the LOS is oriented along the long axis of the eccentric, plunging orbit and the BHs are at pericenter, which corresponds to the smallest projected spatial separation. This has unfortunate implications for attempts to confirm dual BH candidates via spatially-resolved stellar cusps, but it also leads to the important conclusion that some apparently single-core galaxies may in fact be hiding dual BHs at small projected separations. In such cases, other clues may hint at the object's true nature; the yz and xz projections in this example show evidence of disturbed morphology that indicates the galaxy's ongoing merger state. The lower set of stellar density plots in Fig. 5 have a larger field of view, 43 kpc across rather than 15, and have a

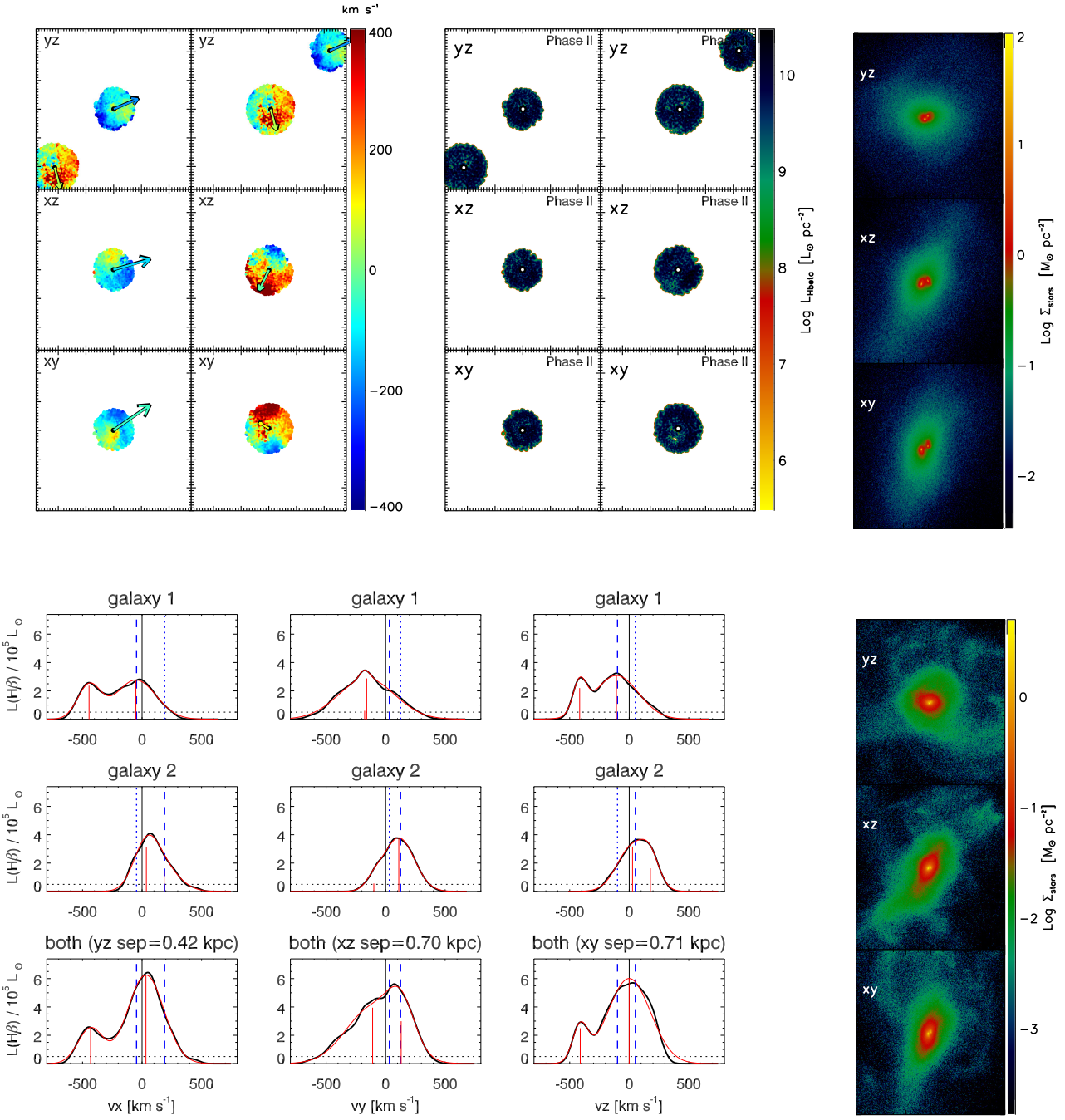

Figure 7. NLR velocity maps, Hβ luminosity maps, and 1-D velocity profiles, as well as stellar density maps, are shown in the same manner as Fig. 5, for a Phase II snapshot in the same ($q = 0.5$, $f_{\rm gas} = 0.3$) simulation. This snapshot occurs 20 Myr prior to BH merger, when the BH separation is 1.1 kpc.

lower minimum density by a factor of 20. In these plots the highly disturbed state of the galaxy is readily apparent in its morphology from each LOS; the wide-field stellar density plots in Figs. 6 & 7 show similarly disturbed morphologies. While disturbed morphology in a dNL AGN host galaxy does not not necessarily indicate a BH pair, as the BHs may have already merged, this signature would establish the system as a late-stage merger, thus removing the possibility of an isolated galaxy or a galaxy with a close, but still widely separated companion. Therefore, sensitive imaging of dNL AGN hosts, for example with *HST*, could aid in distinguishing dual AGN from those with double peaks arising from gas kinematics.

The stellar density plots in Fig. 6 show an example of an unresolved, sub-kpc-scale BH pair that appears as a single density peak. Nonetheless, the galaxy has an asymmetric central stellar structure. The projected BH separation here is much smaller, 170 pc, but in two of the three projections the stellar structure is double-lobed on $\sim$ 10 kpc scales. This reinforces the notion that galaxies with no apparent double-core structure and no disturbed morphology are likely to host dNL AGN arising from pure gas kinematics rather

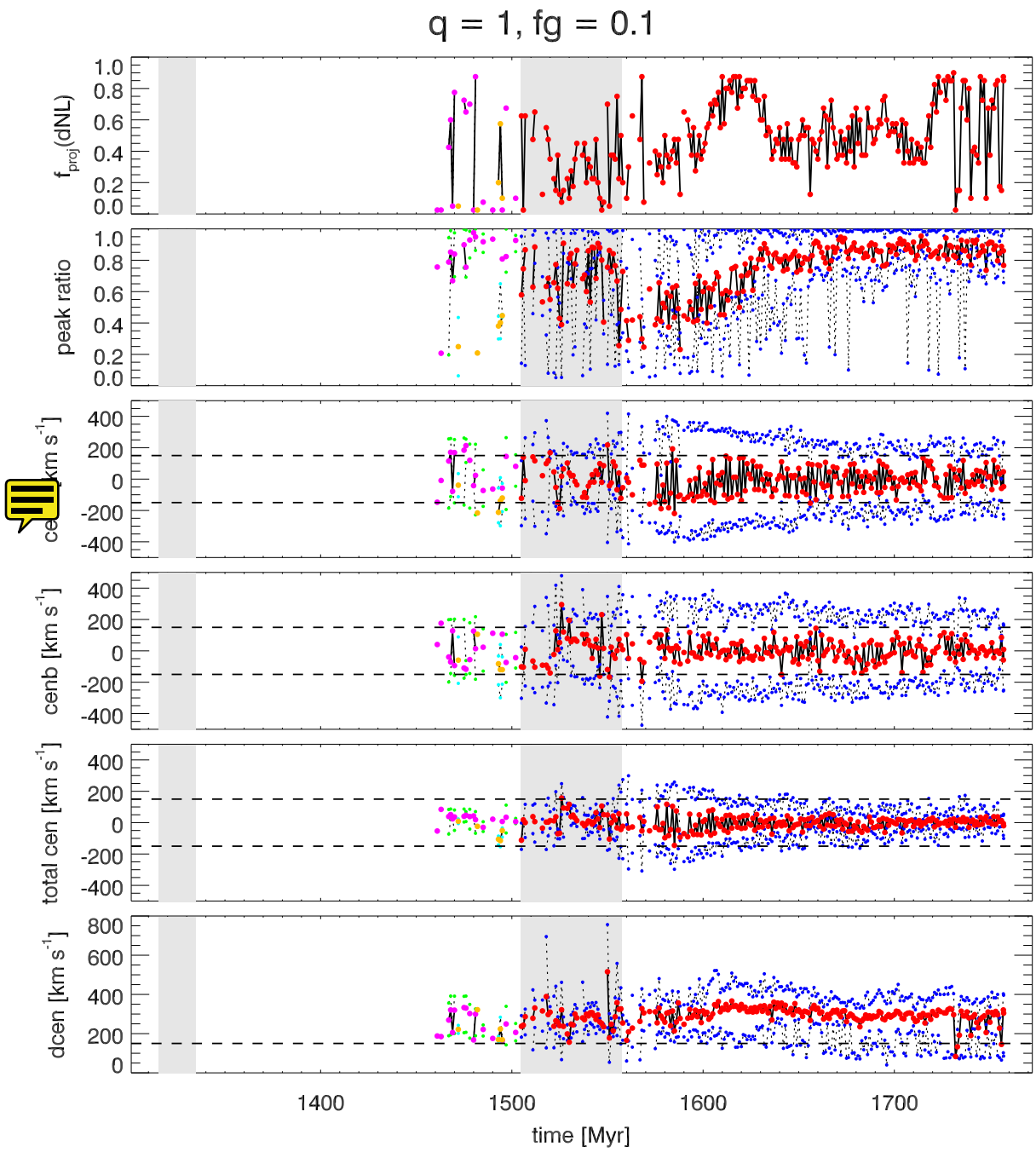

Figure 8. Line-of-sight averaged properties of Hβ velocity profiles versus time. For greater clarity, only the late-merger portion of the simulation is shown, starting 15 Myr before the onset of Phase II. Phase II snapshots are shaded in gray, for $a_{\rm max} = 5.5$ kpc. The simulation shown is an equal-mass merger with $f_{\rm gas} = 0.1$ initially. The top panel shows, as a function of time, the fraction of the 40 random sight lines sampled from which the velocity profile has an observable double peak. "Observable" double peaks are those with a velocity splitting larger than FWHM(a) (corresponding to the brightest peak), a peak ratio larger than 0.05, and a peak $L_{\rm H\beta} > 5 \times 10^4$ L$_\odot$. Only snapshots in which these criteria are met for at least one viewing angle are shown. At times when only one NLR would be seen on a single spectrum (Phases I & IIb), the fraction is shown separately for NLR1 (magenta points) and NLR2 (orange points). In Phases II and III, the fraction is shown for the combined profile (red points). In the other panels, various quantities from the profile fits are shown, averaged over *only* the sight lines for which the profile is double-peaked. The mean values are color-coded as in the top panel, but here the maximum and minimum values are shown as well, in green and cyan, respectively, for NLR1 and NLR2, and in blue for the combined profile. The extremal values are connected with dotted lines while solid lines connect the mean values. Starting with the second panel from the top, the panels show: the peak ratio of the double peaks, the offset of centroid "a", the offset of centroid "b", the offset of the entire profile, and the velocity splitting of the two peaks ($\Delta_{\rm cen}$).

than a dual BH. Our findings do suggest, however, that the absence of two resolvable stellar components does not rule out the presence of a dual AGN, even for spatial resolutions of ~ 1 kpc. Although a candidate dual AGN has recently been found with a separation of 150 pc (Fabbiano et al. 2011), the recent work by Comerford et al. (2011a)—in which all 81 objects observed with slit spectroscopy showed spatially-distinct emission components with separations of at least 200 pc—suggests that sub-kpc-scale dual AGN may be rare. If so, this likely owes to their short lifetimes relative to larger scale pairs. Nonetheless, we suggest that some systems with a single stellar component but with disturbed morphology may contain dual AGN with separations of a few hundred parsec; these may be good candidates for high-resolution *Chandra* (c.f. Fabbiano et al. 2011) or EVLA (c.f. Fu et al. 2011c) observations.

Hβ Profile Diagnostics

Fig. 8 shows the evolution of several line-of-sight averaged quantities for the Hβvelocity profiles in the late-merger stage of an example simulation. This equal-mass merger with initial $f_{\rm gas} = 0.1$ was chosen for illustration because it has sufficient NLR activity to demonstrate all the salient features of the Hβ profiles, but still has a moderate gas content and thus should not be strongly affected by rapid post-merger increases in $v_{\rm esc}$ or by possible dust obscuration. For each snapshot, the data shown are averaged over the projections for which the profile has an observable double peak. Several trends are apparent in these figures. First, both the fraction of random projections from which the profile is double-peaked and the ratio of the two peaks are generally lower and more variable during the kpc-scale phase than during Phases IIb and III. This is because double peaks arising from a single NLR are generally caused by a rotating gas disk in our simulations, whereas some of the double peaks in the kpc-scale phase are caused or influenced by BH motion. In principle, the 1-D velocity profile for two NL AGN in a circular orbit could appear quite similar to that of a rotating disk of the same size. However, the kpc-scale and sub-kpc-scale dual BHs in our simulations generally have plunging, non-circular orbits, and thus appear as double-peaked from a smaller fraction of viewing angles than do the rotating disks. Additionally, we do see a tendency for double peaks in Phases IIb and II (those caused exclusively by rotating gas) to have peak ratios closer to unity than those in the kpc-scale phase. This is the diagnostic proposed by Smith et al. (2011) to differentiate between dNL AGN arising from rotating disks versus dual BHs. While we see that this distinction does exist in an average sense, the peak ratios for the rotating disks in Phases IIb and III still have substantial variation with viewing angle. In the best cases, the peak ratios for a single snapshot range from $\sim 0.6 - 1.0$, while at other times the *mean* peak ratios are $\lesssim 0.5$. Furthermore, in almost every snapshot with an observable double peak, including those in Phase II, the maximum peak ratio is $> 0.8 - 0.9$; i.e., there is usually at least one viewing angle from which the profile has nearly even peaks. We therefore conclude that for individual systems, an uneven-peaked dNL AGN has at most a modestly higher probability of containing a dual BH than one with an even-peaked profile, even for peak ratios as low as $\sim 0.1 - 0.2$.

The velocity splitting of the peaks in each double-peaked profile ($\Delta_{\rm cen}$, bottom panel of Fig. 8) also shows distinct behavior in different merger phases. The spikes in $\Delta_{\rm cen}$ during Phase II in each simulation correspond to pericentric passages of the BHs. Thus, $\Delta_{\rm cen}$ reveals a brief but direct effect of the BH motion on the Hβ velocity profiles, corresponding to times when the BH velocity is maximal. However, the average $\Delta_{\rm cen}$ is as large or larger after the BH merger as during Phase II, owing to the higher gas velocities that reflect a (modest) increase in the depth of the central potential during this time. In general, the NL activity in Phase III is generally longer-lived than in Phase II (see § 3.4), which contributes to the probability of observing a dNL AGN with large $\Delta_{\rm cen}$ in Phase III. In the example shown, however, the largest $\Delta_{\rm cen}$ occur in Phase II; profiles with a maximum $\Delta_{\rm cen} \gtrsim 500$ km s^{-1} occur primarily in Phase II, while lower $\Delta_{\rm cen}$ occur throughout the simulation. We note that in the $q = 1$, $f_{\rm gas} = 0.3$ merger model (the most extreme model used in terms of central gas density and $v_{\rm esc}$), the maximal $\Delta_{\rm cen}$ may be as high as 800 km s^{-1} in the post-merger phase, owing to the large gas velocities in the deep potential well. While obscuration by gas and dust are likely important in such an environment, and may reduce the probability of observing such large velocity splitting in a single NLR, our findings do indicate that it is certainly possible to observe dNL AGN with $\Delta_{\rm cen} > 500$ km s^{-1} arising from a single active BH. Nonetheless, large velocity splittings observed in combination with other evidence for a dual AGN could strengthen the case for the presence of two BHs. Similarly, we calculate the velocity centroid of the entire double-peaked profile (the median velocity of the two peak centroids) and examine phases in which it differs from zero (second panel from bottom in Fig. 8). In principle, a double-peaked profile with a centroid offset from zero could indicate a rotating NLR around one inspiraling BH in a pair, as in Fig. 7. The total offsets are generally less than 150 km s^{-1}, but can briefly reach values of $\sim 300 - 400$ km s^{-1}. Again, there is a correspondence between larger offsets and pericentric passages of the BHs, but such offsets also occur in Phase III owing to some "sloshing" of the recently-merged BH, and the surrounding cusp of gas and stars, in the steepening central potential. It is important to note that even in this case, the offset profile should still reflect motion of the BH, and in real systems, major BH mergers have a high probability of imparting in a GW recoil kick of at least a couple hundred km s^{-1}. At such kick speeds, the BH could retain much of its central cusp and NLR, such that a double-peaked NL profile with an overall offset could result. We do not consider this possibility here, but we note this as an additional possibility for offset dNL profiles. Finally, in our "extreme", $q = 1$, $f_{\rm gas} = 0.3$ merger, the total offsets during Phase III owing to BH sloshing are < 300 km s^{-1} despite the significantly deeper central potential, indicating that this signature has less dependence on the underlying density profile than does the velocity splitting.

ifetimes of Double-NL AGN

Fig. 9 shows the time for which the NLRs have an observable double-peaked profile ($t_{\rm dNL}$) in each merger phase, for eight different galaxy models and for two definitions of Phase II ($a_{\rm max} = 5.5$ and 21 kpc). In each case, the values shown are averages resulting from fitting profiles for 40 random sight lines in each snapshot, and the definitions of merger phases are based on the projected BH separation for each sight line. We can see readily that the definition of Phase II does not affect our results qualitatively, with the exception of the highly-variable Phase IIb. More importantly, the variation in merger phase duration and in $t_{\rm dNL}$ for different values of $a_{\rm max}$ is much less than the variation for different sight lines.

Each bar on the plots in Fig. 9 shows the total phase duration and is subdivided into the total dNL lifetime (magenta) and the total dNL AGN lifetime (green/cyan), according to three different minimum $L_{\rm bol}$ values for defining an AGN. As one might expect, when the Hβ line flux is above the minimum observable criterion, the continuum flux is almost always bright enough to be classified as

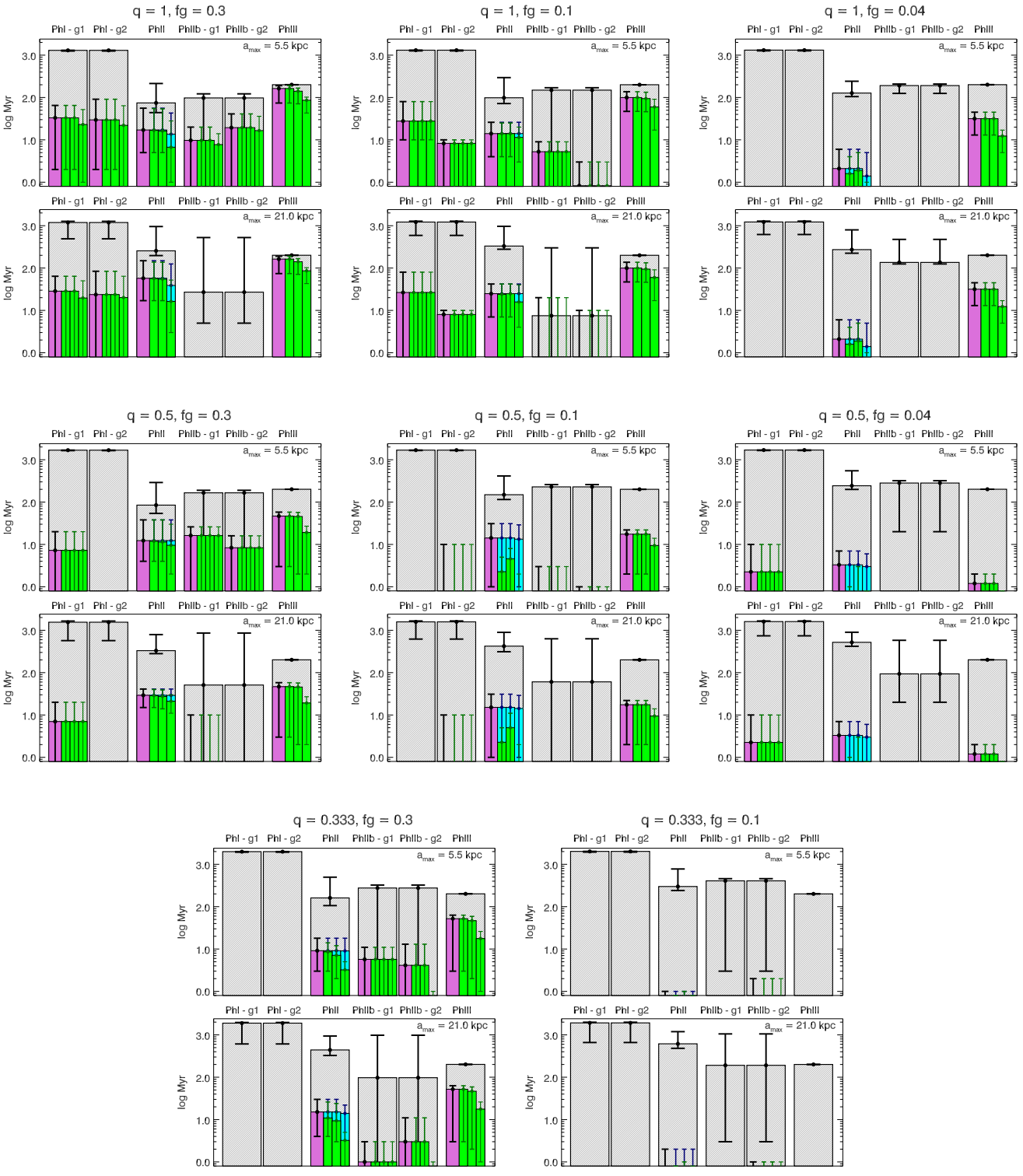

Figure 9. The total time during the merger, separated by merger phase, for which the NLRs have an observable double-peaked profile ($t_{\rm dNL}$). Data are shown for eight simulations with different galaxy models, with q and $f_{\rm gas}$ values as indicated on the plots. The top panel in each plot shows the lifetimes for a kpc-scale phase definition of $a_{\rm max} = 5.5$ kpc, and the bottom panel in each plot is for $a_{\rm max} = 21$ kpc. Within each panel, Phase I is shown in the first two gray bars, separated into galaxy 1 (g1) and galaxy 2 (g2) as during these phases the NLR from each galaxy would not be observable in the same spectrum, followed by Phase II (the kpc-scale phase, as defined in the text), then Phase IIb (g1 & g2) and Phase III. The height of each gray bar represents the mean total duration of each phase averaged over 40 random sight lines (as the phase definitions depend on *projected* BH separation). The error bars give the range of values sampled. Within each large gray bar, the smaller bars are as follows. The magenta bar is the mean lifetime of observable double-peaked NLs ($t_{\rm dNL}$) within each phase, also LOS-averaged with similar error bars. The green and cyan bars denote the mean $t_{\rm dNL}$ for which $L_{\rm bol}$ also exceeds each of our three definitions for AGN luminosity. Specifically, the cyan bars denote when one NLR is active and the other is quiescent, and the green bars denote when both NLRs are active, or when the BHs have merged and only one NLR is present.

an AGN. As this is not true 100% of the time, and because the AGN criteria are free parameters in our analysis, we retain the distinction between a double NL with peak $L_{\mathrm{H}\beta}$ exceeding a minimum luminosity and a double NL AGN that additionally exceeds a minimum L_{bol}.

Comparing t_{dNL} in each phase, we see that in nearly all simulations, Phase III (the post-BH-merger phase) has the longest average t_{dNL}. These lifetimes are typically 10s of Myr, but range from zero to nearly 200 Myr (the total duration of Phase III, at which point we stop the simulation) for the merger models and sight lines shown. Phase II has somewhat shorter dNL lifetimes, typically a few Myr to a few 10s of Myr, but ranging from 0 - 65 Myr. Again, we note that these lifetimes can be considered lower limits on the lifetime of NL emission above the observability threshold, because at times when $L_{\mathrm{H}\beta}$ is slightly below this threshold, the stronger [O III] line may be detectable. In mergers with higher q and f_{gas}, the Phase II definition with $a_{\mathrm{max}} = 21$ kpc results in longer Phase II dNL lifetimes. For the $q = 1$, $f_{\mathrm{gas}} = 0.3$ merger, the increase is a factor of almost three. For mergers with lower q and f_{gas}, however, the Phase II definition has little to no effect on t_{dNL} in Phase II. The duration of Phase IIb, however, is strongly dependent on a_{max} and on the line of sight; along some sight lines it doesnt exist at all, and Phase II spans the entire time between Phases I & III. We see also in Fig. 9 that much of the increase of t_{dNL} in Phase II for $a_{\mathrm{max}} = 21$ versus 5.5 kpc comes from periods defined as Phase IIb via the latter definition. Again, this variation in the relative duration of Phases II and IIb is substantially smaller than the fundamental uncertainty caused by viewing-angle dependence.

t_{dNL} for Phase I is also somewhat variable, but is usually shorter than t_{dNL} for Phase II. This is contrary to what one might naively assume, because the total duration of Phase I is quite long, in excess of 1 Gyr. As discussed in § 3.1, L_{bol} and $L_{\mathrm{H}\beta}$ peak first during Phase I (after the first pericentric passage of the galaxies) and again during Phases II & III (during final coalescence). Although L_{bol} is Eddington-limited for a brief time during each peak, the Eddington limit is nearly ten times higher during coalescence, owing to the BH growth in the meantime. Accordingly, the NLRs are also generally less luminous during Phase I and the lifetime of observable double-peaked NLs is shorter, despite the fact that the *total* duration of Phase I is much greater than the combined duration of Phase II and Phase III.

As mentioned in § 3.1.1, the peak of AGN and NL activity usually occurs near the time of the BH merger. This means that *double NL activity is likely to be associated with impending or recent BH mergers*. However, as discussed in § 3.1.2, mergers with lower q and f_{gas} have lower AGN and NL activity overall, and we see the consequences of this strong dependence of dNL AGN lifetimes on q and f_{gas} in Fig. 9. The merger with $q = 0.333$ and initial $f_{\mathrm{gas}} = 0.1$, which is still a major merger, has almost no double NL AGN in any merger phase.

In short, for mergers with non-negligible NL activity, the time from the kpc-scale phase of BH inspiral through the first few hundred Myr after the BH merger is the phase in which double NL AGN (and NL AGN in general) are most likely to be observable. The relative dNL AGN lifetimes in Phase II and Phase III depend on exactly when the AGN emission peaks relative to the time of BH merger, and on other factors such as the ratio of Hβ luminosities from each NLR prior to merger. However, the tendency for dNL AGN to be observable in the late merger stage occurs *regardless* of whether the double-peaked profiles are a direct result of BH motion or are simply a result of NLR kinematics. Thus, "serendipitous" discoveries of dual AGN with double-peaked profiles, but in which the double peak results from gas kinematics (cf. Fu et al. 2011b), are to be expected as a consequence of the timing of the kpc-scale phase relative to the peak of AGN activity.

4 DISCUSSION

We have conducted a study of the narrow-line AGN signatures of single and dual BHs in merging galaxies. A key component of this endeavour was the development of the first model for narrow-line emission from AGN in full hydrodynamic simulations of evolving, interacting galaxies. Our model was applied to the output of SPH (GADGET-3) simulations of merging galaxies with central, accreting BHs, allowing us to obtain velocity profiles for Hβ emission for arbitrary sight lines, throughout the galaxy merger. While this approach represents only a first attempt to understand the complex dynamical and radiative processes in the centers of merging galaxies, our work highlights several generic trends in the kinematics and luminosity of photoionized gas around BHs during such events. When combined with further information regarding, for example, the underlying stellar distribution and the bolometric (continuum) AGN luminosity, these results can inform the prospects for confirming candidate dual BHs with future follow-up observations of double-peaked NL AGN.

4.1 Evolution and Kinematics of Double-Peaked Narrow-Line AGN

The kpc-scale phase of BH evolution in a major galaxy merger lasts up to a few hundred Myr, while the merger itself takes $\sim 1-2$ Gyr from first infall to final coalescence. Within the kpc-scale phase (Phase II in the above discussion), the BHs have observable double-peaked NL AGN profiles for only a fraction of the time; the dNL AGN lifetimes in Phase II range from < 1 Myr to a few tens of Myr. Thus, dNL AGN seem to be a generic but relatively short-lived feature of major, gaseous mergers.

We also find that NL AGN have relatively low luminosities during the early phase of galaxy merging (Phase I in the above discussion). Therefore, most of the observable NL emission triggered by major mergers should occur in the late stages of merging, during the final coalescence of the two galaxies. This is precisely the phase when kpc-scale or smaller BH pairs should form and merge. Thus, owing to this coincidence in timing, dNL AGN triggered by major mergers are most likely to be associated with approximately-kpc-scale BH pairs or with recent BH mergers (Phase III in the above discussion).

Follow-up observations of dNL AGN indicate that a minority of these objects show evidence for dual BHs; the rest of the double-peaked features are either ambiguous or are presumed to result from gas kinematics. If a substantial fraction of dNL AGN were *directly* associated with kpc-scale BH pairs, our results would be in tension with this finding. However, we find that only a *minority* of dNL AGN result directly from BH motion, *even within the kpc-scale phase of BH evolution*. The canonical picture in which double peaks arise from two distinct NLRs orbiting about a common central potential is only one of several possible mechanisms, and it is not the most common. If the BH separation is comparable to the size of the NLRs, then double peaks may arise from the direct interaction of the BHs with the NL gas. In other cases, a double-peaked feature may arise from a single NLR, but may be *influenced* by the relative BH motion. For example, an offset peak in one NLR may alter the peak ratio of the observed profile, and

it may cause the dNL profile to be offset from the rest frame of the host galaxy. However, many dNL AGN are simply *coincident* with the kpc-scale phase, and arise purely from gas kinematics in a single NLR. This is consistent with the minority of dNL AGN that show good evidence of association with dual BHs, even if every dNL AGN occurs in a late stage galaxy merger. Our findings also indicate that the serendipitous discoveries of dual AGN, in which the double-peaked profiles are unassociated with the two BHs (Fu et al. 2011b), could in fact be a relatively common occurrence for merger-triggered dNL AGN. In our simulations, we find that dNL AGN induced directly by BH motion generally account for a minority of the double-peaked profiles in the kpc-scale phase, with few occurring for BH separations > 5.5 kpc. However, the fraction of double-peaked profiles in Phase II that are influenced by BH motion either directly or indirectly is typically $> 50\%$, at least when Phase II is defined for BH pairs with $a_{\rm sep} < 5.5$ kpc. The remainder of double-peaked NLs mostly arise from rotating gas disks, though up to $\sim$ 20-30% of profiles in Phase II initially classified as double peaks are actually complex (multi-peaked) or highly-asymmetric profiles arising from disturbed or superimposed NL emission regions. Finally, we note that our thermal feedback model for AGN does not allow for the consideration of AGN outflows or jets, which may be additional mechanisms for producing double-peaked NLs, though they may be distinguishable compact emission regions. Rosario et al. (2010) have demonstrated that some jets may be resolved via radio imaging. Comerford et al. (2011a) have similarly suggested that AGN with spatially-extended emission components possibly caused by outflows are less-compelling dual BH candidates, though the possibility of a dual AGN with outflows cannot be excluded.

Additionally, the observed kinematic features of NL AGN are strongly dependent on viewing angle. Our results for the occurrence of double-peaked NLs therefore have a fundamental uncertainty owing to the possible range of sight lines. To account for this, we fit velocity profiles and calculate dNL AGN lifetimes for many lines of sight in each simulation snapshot. The LOS variation in dNL AGN lifetimes is substantial, typically at least an order of magnitude. This further supports the idea that many dual AGN with NL activity may not show a clear association with a double-peaked profile.

The amount of dNL AGN activity during the merger also shows strong dependence on the conditions in the merging galaxies, owing largely to variation in the BH accretion rates. Specifically, more AGN and NL activity occurs in mergers with higher mass ratio (closer to equal mass) and gas content, i.e. those that create the strongest inflow of gas to the central galactic regions. Second-order effects steepen this trend somewhat, as discussed in § 3.1.2. Other possibly relevant parameters were also considered, including the orbits of the merging galaxies and the presence of a stellar bulge in the progenitors; however, the variation in NL activity for these parameters is much smaller than for the mass ratio and gas fraction, and it is also smaller than the intrinsic LOS variation.

4.2 Additional Signatures of Dual AGN

dNL AGN in which two brightness peaks can be resolved in imaging and are spatially coincident with the NL emission components can be considered strong dual BH candidates. Accordingly, we examine the stellar distribution in our simulated merging galaxies. After the burst of star formation following the first close passage of the galaxies, each BH is surrounded by a dense cusp of stars and gas; regardless of the AGN luminosity, these cusps should appear as two brightness peaks with sufficient spatial resolution. However, many dNL AGN induced by BH motion have projected BH separations less than a kpc and may be difficult to resolve. Therefore, there may be a significant population of dNL AGN that do not show clear association with a BH pair, even though a pair is present. Other means must be employed to confirm the presence of a dual BH in such systems.

Some additional information may be obtained from sensitive, high-resolution (i.e., *HST*) imaging of the large-scale galactic morphology. If the galaxy appears undisturbed, or if it shows obvious signs of being in an early-merger phase (for example, two widely-separated galaxies, perhaps with characteristic tidal bridge and tail features), a kpc-scale dual AGN would be disfavored. If a kpc-scale BH pair is present, the galaxy should appear as a late-stage merger remnant, i.e. a single galaxy that is morphologically disturbed. However, because the galactic morphology should appear much the same after the BHs have merged, this diagnostic cannot rule out a post-BH-merger (Phase III) dNL AGN.

Smith et al. (2011) have suggested that dNL AGN with even-peaked profiles are less likely to be dNL AGN, on the grounds that rotating gas disks should have double-peaked profiles with roughly even peaks, and that BHs are unlikely to have very similar luminosities. We do see a trend toward higher peak ratios (closer to unity) for double-peaked NLs arising from rotating gas disks around a single BH than for dNL AGN in the kpc-scale phase of BH pair evolution. However, in the single-NLR case the peak ratios still vary substantially, and in the dual-BH case there is almost always at least one viewing angle for which the double-peaked profile has nearly even peaks. Thus, dNL AGN with uneven peak ratios < 0.5 should have a higher probability of containing a dual BH, but this increase may be small and is difficult to predict for a given source or sample of sources.

We also find that large velocity splittings in double-peaked profiles are often, but not exclusively, associated with the kpc-scale phase. Velocity splittings increase during pericentric passages of the BHs, reflecting the impact of BH motion on the velocity profiles. However, in the nearly-equal-mass, gas-rich mergers in which the central escape speed increases around the time of the merger, the larger gas velocities in the central cusp also increase the velocity splitting for rotating gas in a single NLR. Large peak separations may also occur in AGN with high-velocity outflows, though these cases should be more easily distinguishable as spatially-extended emission components. Thus, dNL AGN with spatially-compact emission components separated by $\gtrsim 500 - 600$ km s^{-1} may be good candidates for hosting a dual AGN, though some of these may be single rotating NLRs in gas-rich merger remnants. Another possible signature of double-peaked profiles associated with dual BHs is an overall velocity offset of the profile, which could arise from a single, rotating NLR around an inspiralling BH. Again, this signature could also arise from a recently-merged BH if it sloshes though the central region before settling down, especially as BHs may often receive GW recoil kicks $\gtrsim 100 - 200$ km s^{-1}. In any case, our results indicate that dNL AGN with discernible overall velocity offsets are likely to be associated with BH motion of some kind, and that these systems have a somewhat higher probability of containing dual BHs.

4.3 Model Assumptions and Prospects for Future Work

The qualitative picture outlined in this initial study of the kinematics of NL gas in major galaxy mergers is insensitive to the choice of parameters for our simulations and semi-analytical model. How-

ever, the quantitative results do have some dependence on the model parameters. The variation in our results with these parameters is in general smaller than the intrinsic variability with viewing angle, and we have chosen these parameters such that our simulated NLRs broadly reproduce the size and luminosity of observed NL AGN. Here we discuss this model dependence in more detail, as well as possibly relevant physics to be included in future work.

As discussed in § 3.1.2, our results have some quantitative dependence on the gas EOS used; softer EOS models result in more stable gas disks, and thus less AGN and NL activity. Qualitatively, we find that a nearly-isothermal EOS (softened EOS parameter $q_{\rm EOS} = 0.05$) results in higher sustained accretion rates following the initial close passage of the galaxies and preferentially more NL activity in the early merger phase.

Our results are generally independent of the choice of mass and spatial resolution, though we do require that the NLRs be at least marginally resolved in order to impart physical meaning to these results. By conducting a small resolution study we do find a weak trend toward higher central densities and accretion rates for higher resolution, but this has little effect on our results. In particular, despite slight variations in our calculated AGN lightcurves and peak luminosities, the total amount of accretion remains constant regardless of resolution.

Without arbitrarily high resolution, we cannot exclude the possibility that gas kinematics on sub-resolution scales could shape the resulting velocity profiles in an unpredictable manner. However, this will only affect double-peaked profiles arising from gas kinematics, and it is possible that turbulent motion in rotating NLRs would smear out some of these double peaks, thereby increasing the fraction of dNL AGN caused by BH motion. We can robustly predict that at least for a small fraction of the kpc-scale (and sub-kpc scale) phase, the NL gas kinematics will be dominated by the BH motion, regardless of the gas motion on sub-resolution scales.

A related issue is the extent to which our NL models are limited by the multi-phase ISM treatment of Springel & Hernquist (2003). While this model has shown success in reproducing the global properties of merging galaxies (e.g., Cox et al. 2006; Hopkins et al. 2006), its treatment of gas physics on small scales is necessarily highly simplified. For example, if stellar feedback drives strong turbulence, then the assumed pressure equilibrium between hot and cold gas phases would be violated. Future work that relies on a turbulent-pressure-driven ISM model will produce more realistic distributions of gas density and temperature, allowing a more accurate identification of the NL-emitting gas.

Perhaps the most important caveat to the work presented here is the lack of obscuring dust in our models. While we do account for self-shielding of NL clouds in an average sense, such that AGN continuum photons are not double-counted, our models do not include radiative transfer calculations and thus are unable to account for the effects of dust obscuration. We accordingly restrict our analysis to galaxies with relatively low initial gas fractions, as higher gas fractions generally drive stronger starbursts and produce much more dust. Starbursts can additionally produce substantial NL emission from stellar photoionization, which is also not accounted for in our model. The results from models with initial gas fractions of 30%, the highest included in this study, are to be considered less robust in this sense. However, we note that in cases where the dust and gas have a clumpy distribution, such that the central galactic region is only partially obscured, it is likely that double-peaked features arising from kinematics in a single NLR would be preferentially removed by dust reprocessing. Double peaks arising from the relative motion of two spatially-separated NLRs may be more likely to survive, thus strengthening the correlation between dNL AGN and dual BHs. The incorporation of full radiative transfer calculations in future work, including models for dust and stellar photoionization, will allow a more direct comparison of numerical results to observed AGN.

4.4 Broader Implications

It is important to note that all of the analysis presented here applies only to AGN triggered by major galaxy mergers. We therefore cannot comment on the contribution of AGN triggered by minor mergers or secular processes to the population of double-peaked NL objects. More generally, a strong consensus on the fraction of AGN triggered by mergers does not currently exist, as surveys with different selection criteria have obtained widely disparate results (e.g., Cisternas et al. 2011; Ellison et al. 2011; Koss et al. 2011b).

The scenario conceived to motivate searches for dual BHs in double-peaked NL AGN—i.e. two well-separated, observable NLRs in relative motion—has been shown to occur for only a small fraction of the kpc-scale phase. Observations indicate that a minority of dNL AGN show clear evidence of association with dual brightness peaks in imaging. Therefore, we may ask the question of whether double-peaked NL signatures are a good tool for identifying dual BHs. In relative terms, studies of dNL AGN have certainly proved to be an *effective* means of finding good dual BH candidates; the number of good candidates identified through follow-up observations has greatly increased the known population of these objects. Less clear is whether observing dNL AGN is an *efficient* means of identifying dual BHs. We have demonstrated that even within the kpc-scale phase, a wide variety of gas and BH configurations may give rise to double-peaked features. However, our results also indicate that for merger-triggered AGN, dNL AGN are most likely to be observed during the late stages of the merger, either shortly before or shortly after the BHs themselves merge. Thus, many dNL AGN that do not contain dual BHs may be associated with recent BH mergers, which is interesting in its own right. As mentioned above, BH mergers should result in a GW recoil kick, which in many cases may be $\gtrsim 100-200$ km s^{-1}. At these velocities, the BH may retain much of its cusp of gas and stars, such that the BH motion, while short-lived, could possibly be detected as a *narrow-line* offset in the AGN spectrum. At larger velocities that could displace the BH significantly from the center of the galaxy ($\gtrsim 500-1000$ km s^{-1}), only the accretion disk would be remain bound to the BH, and the material at larger radii would be left behind. This would result in the offset *broad line* signature that is more commonly considered for recoiling BHs (e.g., Loeb 2007; Blecha et al. 2011), and in such cases the post-BH-merger phase clearly would not contribute to the dNL AGN lifetime.

The finding that many double-peaked features are produced by sub-kpc-scale BH pairs, as well as the sensitive dependence of dNL AGN lifetimes on viewing angle, indicates that many of the currently "ambiguous" dNL AGN candidates may in fact contain dual BHs. A critical observation from our results is that regardless of the degree of *causation* of dNL AGN by dual BHs, a *correlation* in the timing of their occurrence does exist. Furthermore, as described above, some of the physics not accounted for in our current models could possibly increase the fraction of dNL AGN induced by BH motion relative to those induced by gas kinematics. Thus, we conclude that continued dedicated, multi-wavelength follow-up observations of dNL AGN should reveal a larger population of strong candidate BH pairs. Furthermore, multiple lines of indirect

evidence, including the signatures discussed in this work, should be combined to determine the most promising dual BH candidates.

ACKNOWLEDGEMENTS

REFERENCES

Baker J. G., Centrella J., Choi D.-I., Koppitz M., van Meter J., 2006, Phys. Rev. Lett., 96, 111102

Begelman M. C., Blandford R. D., Rees M. J., 1980, Nature, 287, 307

Berczik P., Merritt D., Spurzem R., Bischof H.-P., 2006, ApJ, 642, L21

Bianchi S., Chiaberge M., Piconcelli E., Guainazzi M., Matt G., 2008, MNRAS, 386, 105

Blecha L., Cox T. J., Loeb A., Hernquist L., 2011, MNRAS, 412, 2154

Bogdanović T., Eracleous M., Sigurdsson S., 2009, ApJ, 697, 288

Bondi H., Hoyle F., 1944, MNRAS, 104, 273

Boroson T. A., Lauer T. R., 2009, Nature, 458, 53

Campanelli M., Lousto C. O., Marronetti P., Zlochower Y., 2006, Phys. Rev. Lett., 96, 111101

Cisternas M., Jahnke K., Inskip K. J., Kartaltepe J., Koekemoer A. M., Lisker T., Robaina A. R., Scodeggio M., Sheth K., Trump J. R., Andrae R., Miyaji T., Lusso E., Brusa M., Capak P., Cappelluti N., Civano F., Ilbert O., Impey C. D., Leauthaud A., Lilly S. J., Salvato M., Scoville N. Z., Taniguchi Y., 2011, ApJ, 726, 57

Comerford J. M., Gerke B. F., Newman J. A., Davis M., Yan R., Cooper M. C., Faber S. M., Koo D. C., Coil A. L., Rosario D. J., Dutton A. A., 2009, ApJ, 698, 956

Comerford J. M., Gerke B. F., Stern D., Cooper M. C., Weiner B. J., Newman J. A., Harrison F., Madsen K., Barrows R. S., 2011a, ArXiv e-prints

Comerford J. M., Pooley D., Gerke B. F., Madejski G. M., 2011b, ApJ, 737, L19

Cox T. J., Dutta S. N., Di Matteo T., Hernquist L., Hopkins P. F., Robertson B., Springel V., 2006, ApJ, 650, 791

Di Matteo T., Springel V., Hernquist L., 2005, Nature, 433, 604

Dotti M., Montuori C., Decarli R., Volonteri M., Colpi M., Haardt F., 2008, ArXiv e-prints

Ellison S. L., Patton D. R., Mendel J. T., Scudder J. M., 2011, MNRAS, 418, 2043

Eracleous M., Boroson T. A., Halpern J. P., Liu J., 2011, ArXiv e-prints

Escala A., Larson R. B., Coppi P. S., Mardones D., 2004, ApJ, 607, 765

Fabbiano G., Wang J., Elvis M., Risaliti G., 2011, Nature, 477, 431

Fu H., Myers A. D., Djorgovski S. G., Yan L., 2011a, ApJ, 733, 103

Fu H., Yan L., Myers A. D., Stockton A., Djorgovski S. G., Aldering G., Rich J. A., 2011b, ArXiv e-prints

Fu H., Zhang Z.-Y., Assef R. J., Stockton A., Myers A. D., Yan L., Djorgovski S. G., Wrobel J. M., Riechers D. A., 2011c, ArXiv e-prints

Gerhard O. E., Binney J., 1985, MNRAS, 216, 467

Gould A., Miralda-Escude J., 1997, ApJ, 483, L13+

Green P. J., Myers A. D., Barkhouse W. A., Mulchaey J. S., Bennert V. N., Cox T. J., Aldcroft T. L., 2010, ArXiv e-prints

Hennawi J. F., Strauss M. A., Oguri M., Inada N., Richards G. T., Pindor B., Schneider D. P., Becker R. H., Gregg M. D., Hall P. B., Johnston D. E., Fan X., Burles S., Schlegel D. J., Gunn J. E., Lupton R. H., Bahcall N. A., Brunner R. J., Brinkmann J., 2006, AJ, 131, 1

Hopkins P. F., Hernquist L., Cox T. J., Di Matteo T., Robertson B., Springel V., 2006, ApJS, 163, 1

Komossa S., Burwitz V., Hasinger G., Predehl P., Kaastra J. S., Ikebe Y., 2003, ApJ, 582, L15

Koss M., Mushotzky R., Treister E., Veilleux S., Vasudevan R., Miller N., Sanders D. B., Schawinski K., Trippe M., 2011a, ApJ, 735, L42

Koss M., Mushotzky R., Veilleux S., Winter L. M., Baumgartner W., Tueller J., Gehrels N., Valencic L., 2011b, ApJ, 739, 57

Liu X., Greene J. E., Shen Y., Strauss M. A., 2010a, ApJ, 715, L30

Liu X., Shen Y., Strauss M. A., Greene J. E., 2010b, ApJ, 708, 427

Loeb A., 2007, Physical Review Letters, 99, 041103

McGurk R. C., Max C. E., Rosario D. J., Shields G. A., Smith K. L., Wright S. A., 2011, ApJ, 738, L2

Mihos J. C., Hernquist L., 1996, ApJ, 464, 641

Milosavljević M., Merritt D., 2001, ApJ, 563, 34

Osterbrock D. E., Ferland G. J., 2006, Astrophysics of gaseous nebulae and active galactic nuclei, Osterbrock, D. E. & Ferland, G. J., ed.

Pretorius F., 2005, Phys. Rev. Lett., 95, 121101

Robertson B., Bullock J. S., Cox T. J., Di Matteo T., Hernquist L., Springel V., Yoshida N., 2006, ApJ, 645, 986

Rodriguez C., Taylor G. B., Zavala R. T., Peck A. B., Pollack L. K., Romani R. W., 2006, ApJ, 646, 49

Rosario D. J., McGurk R. C., Max C. E., Shields G. A., Smith K. L., Ammons S. M., 2011, ApJ, 739, 44

Rosario D. J., Shields G. A., Taylor G. B., Salviander S., Smith K. L., 2010, ApJ, 716, 131

Shen Y., Liu X., Greene J. E., Strauss M. A., 2011, ApJ, 735, 48

Smith K. L., Shields G. A., Bonning E. W., McMullen C. C., Rosario D. J., Salviander S., 2010, ApJ, 716, 866

Smith K. L., Shields G. A., Salviander S., Stevens A. C., Rosario D. J., 2011, ArXiv e-prints

Springel V., 2005, MNRAS, 364, 1105

Springel V., Di Matteo T., Hernquist L., 2005, MNRAS, 361, 776

Springel V., Hernquist L., 2003, MNRAS, 339, 289

Tsalmantza P., Decarli R., Dotti M., Hogg D. W., 2011, ApJ, 738, 20

Yu Q., 2002, MNRAS, 331, 935